INVESTIGATION OF PRESSURE DISTRIBUTION IN PIPELINE FOR TRANSPORTATION OF COAL ASH SLURRY

A Thesis Report Submitted
in partial fulfillment of the requirements for
the award of degree of

MASTER OF ENGINEERING
IN
THERMAL ENGINEERING

Submitted by

RANJAN CHAUDHARY
Roll No.: 801083023

Under the Guidance of

Mr. Satish Kumar
Department of Mechanical Engineering
Thapar University, Patiala.

Dr. Dwarika Nath Ratha
Department of Civil Engineering
Thapar University, Patiala.

DEPARTMENT OF MECHANICAL ENGINEERING
THAPAR UNIVERSITY
PATIALA-147004, INDIA.

June 2012

DECLARATION

I hereby declare that the work which is being presented in the dissertation work entitled, **"Investigation of pressure distribution in pipeline for transportation of coal ash slurry"**, in partial fulfillment of the requirements for the award of degree of Master of Engineering in Mechanical Engineering with specialization in **Thermal Engineering** submitted in Mechanical Engineering Department of Thapar University, Patiala, is an authentic record of my own work carried out under the supervision of **Mr. Satish Kumar (Assistant Prof. MED) and Dr. Dwarika Nath Ratha (Assistant Prof. CED)** refers other researcher's works which are duly listed in the reference section.

The matter presented in this thesis has not been submitted for the award of any other degree of this or any other university.

Ranjan Chaudhary

This is to certify that the above statement made by the candidate is correct and true to the best of my knowledge.

Mr. Satish Kumar
Assistant Professor, MED
Thapar University, Patiala

Dr. Dwarika Nath Ratha
Assistant Professor, CED
Thapar university, Patiala

Counter signed by

Dr. Ajay Batish
Professor & head
Mechanical Engineering Department
Thapar University, Patiala

Dr. S.K. Mohapatra
Dean of Academic Affairs
Thapar University, Patiala

ACKNOWLEDGEMENTS

Words are often less to revels one's deep regards. With an understanding that work like this can never be the outcome of a single person, I take this opportunity to express my profound sense of gratitude and respect to all those who helped me through the duration of this work.

This work would not have been possible without the encouragement and able guidance of supervisor Mr. Satish Kumar and Dr. Dwarika Nath Ratha. Their enthusiasm and optimism made this experience both rewarding and enjoyable. Most of the novel ideas and solutions in this work are the result of our numerous stimulating discussions. Their feedback and editorial comments were also invaluable for the writing of this thesis.

I take pride of myself being son of ideal parents for their everlasting desire, sacrifice, affectionate blessings, and help, without which it would not have been possible for me to complete my studies.

I am also very grateful to my all friends and colleague (Sukhdeep Singh and Aman Sharma) for accompanying me during the most outstanding year of my life and standing by me in every situation.

I would like to thank to all the faculty members and employees of Mechanical Engineering Department, Thapar Univeristy, Patiala for their everlasting support.

Last but not least, I would like to thank God for all good deeds.

(Ranjan Chaudhary)

ABSTRACT

Slurry transportation system has been used in thermal power plants for the transporation of bottom ash. This system has proved its efficient working and advantages such as less noisy, no air pollution. But still now optimization is required for better performance. In the present work rheological properties of various bottom and fly ash mixtures are studied to evaluate the factors affecting the flow behaviour of slurry. Bottom and fly ash for the present investigation was collected from the Guru Gobind Singh thermal power plant, Ropar. Particle size distribution, pH , settling characteristics of bottom and fly ash are investigated. Rheometer is used for the shear rate and shear stress variation for the different ratios of bottom and fly ash.

Numerical simulation is performed on the slurry flow through straight pipe and 90^0 horizontal bend for the evaluation of pressure drop per unit length. Modeling of Straight pipe and 90^0 horizontal bend is performed in Gambit version 2.2, Fluent version 6.2 is used for the numerical evaluation. Simulation has been performed on various concentrations(20%,30%,40% & 50%) of bottom and fly ash mixtures varying flow velocity from 1.5m/s to 3m/s. It is found that pressure drop increases with increasing flow velocity and higher concentrations(by weight) of bottom and fly ash mixtures.

CONTENTS

LIST OF FIGURES

Nomenclature and abbreviations

Symbol	Description	Dimensions
ρ	Density	kg/m^3
t	Time	Second
p	Pressure	Pascal
v	Velocity	m/s
z	Datum height	m
g	Gravity	m/s^2
CFD	Computational Fluid Dynamics	
%	Percentage	
A	Area	m^2
D	diameter	m
H_l	Head loss	m
L	Length	m
B.A	Bottom ash	
F.A	Fly ash	

CHAPTER 1

INTRODUCTION

Transportation of some materials through slurry transportation system proved a much better means of material transport. One of the best examples is the transport of bottom ash through slurry pipelines in thermal power plants. There are various advantages of slurry transport system such as very less pollution less and less noise. Therefore, due to its well response and good characteristics, detailed study is needed to improve its functioning for better performance**.**

1.1 SLURRY

A slurry is a thin sloppy mud or cement or, in extended use, any fluid mixture of a pulverized solid with a liquid (usually water), often used as a convenient way of handling solids in bulk. Slurries behave in some ways like thick fluids, flowing under gravity and being capable of being pumped. The physical characteristics of slurry are dependent on many factors such as particle size and distribution, solid concentration in the liquid phase, turbulence level, temperature, conduit size, and viscosity of the carrier. Slurry is a mixture of a solid particles and fluid held in suspension. Water is the most commonly used fluid. Theoretically, for laminar to a turbulent flow a single-phase liquid of low absolute (or dynamic) viscosity can be allowed to flow at slow speeds. However, slurry which is two-phase mixture must overcome a deposition critical velocity or a viscous transition critical velocity. The speed of slurry flow is sufficiently high to maintain the particles in suspension. The mixture resists the flow in highly viscous mixtures because of excessively low shear rate in the pipeline.

1.1.1 Types of Slurry Flows

There are two types of slurry flows:

i. Homogeneous flow
ii. Heterogeneous flow

Homogeneous Flows

The solids are uniformly distributed in the liquid carrier in homogeneous flow. The Particle size is less than 60-100μm. For example copper concentrate slurry after undergoing a process of grinding and thickening, Drilling mud, sewage sludge, and fine limestone behave as homogeneous flows.

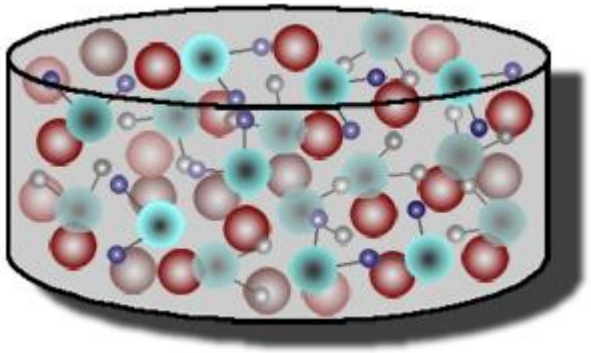

Figure 1.1: Homogeneous mixture

Heterogeneous flows

The solids are not uniformly mixed in the horizontal plane in heterogeneous flow. The particle size is greater than 100μm. Heavier particles settle down at the bottom and lighter particles float in suspension in heterogeneous flow. This forms the sliding bed in the pipe. Heterogeneous slurries are encountered in many places like mining and dredging applications. Minimum carrier velocity is required for heterogeneous flow.

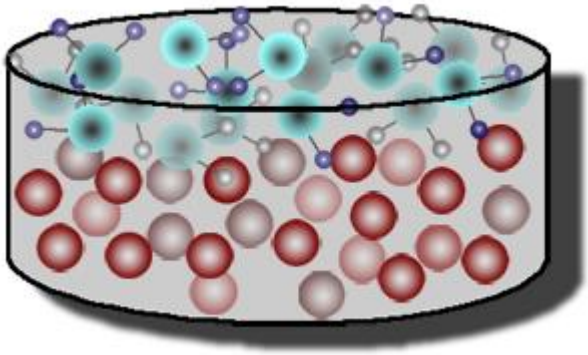

Figure 1.2: Heterogeneous mixture, partly stratified.

1.2 THERMAL POWER PLANT ASH

Ash coming out after the combustion of pulverized coal in thermal power plants are divided into two main categories: Fly ash and Bottom ash.

1.2.1 Fly Ash

Fly ash is one of the residues generated in combustion, and comprises the fine particles that rise with the flue gases .In an industrial context, fly ash usually refers to ash produced during combustion of coal. Fly ash is generally captured by electrostatic precipitators or other particle filtration equipment before the flue gases reach the chimneys of coal-fired power plants, the components of fly ash vary considerably, but all fly ash includes substantial amounts of silicon dioxide (SiO_2) (both amorphous and crystalline) and calcium oxide (CaO), both being endemic ingredients in many coal-bearing rock strata.

Two classes of fly ash are defined as: **Class F fly ash** and **Class C fly ash**. The chief difference between these classes is the amount of calcium, silica, alumina, and iron content in the ash. The chemical properties of the fly ash are largely influenced by the chemical content of the coal burned

Class F Fly Ash

The burning of harder, older anthracite and bituminous coal typically produces Class F fly ash. This fly ash is pozzolanic in nature, and contains less than 20% lime (CaO).

Class C Fly Ash

Fly ash produced from the burning of younger lignite or sub bituminous coal, in addition to having pozzolanic properties, also has some self-cementing properties. In the presence of water, Class C fly ash will harden and gain strength over time. Class C fly ash generally contains more than 20% lime (CaO). Unlike Class F, self-cementing Class C fly ash does not require an activator. Alkali and sulphate (SO_4) contents are generally higher in Class C fly ashes.

1.2.2 Bottom Ash

Main components of bottom ash are Nickel, Chromium, arsenic Lead and Sulphur. Bottom ash from the pulverized power plants consists of granular particles with a minor input of melted glassy fragments, while the bottom ash from the fluidized bed combustor consists entirely of granular particles. The sulphur and carbon contents of pulverized bottom ashes range from 0.03 to 2.32 weight % and 0.19 to 6.62 weight %, respectively. For the fluidized bed combustor, the sulphur and carbon contents were 5.27 wt % and 10.72 weight %. The concentrations of As, Cr, Hg, Ni, and Pb in bottom ash are related to sulphur content of coal and are higher for bottom ashes from high sulphur feed coals.

1.3 ASH HANDLING SYSTEM:

The ash handling system handles the ash by bottom ash handling system, coarse ash handling system, fly ash handling system, ash disposal system up to the ash disposal area and water recovery system from ash pond and Bottom ash overflow. Description is as follows:

1.3.1 Bottom Ash Handling System

Bottom ash resulting from the combustion of coal in the boiler shall fall into the over ground, refractory lined, water impounded, maintained level, double V-Section type/ W type steel-fabricated bottom ash hopper having a hold up volume to store bottom ash and economizer ash of maximum allowable condition with the rate specified. The slurry formed shall be transported to slurry sump through pipes.

1.3.2 Coarse Ash (Economizer Ash) handling System

Ash generated in Economizer hoppers shall be evacuated continuously through flushing boxes. Continuous generated Economizer slurry shall be fed by gravity into respective bottom ash hopper pipes with necessary slope.

1.3.3 Air Pre Heater ash handling system

Ash generated from air pre heater hoppers shall be evacuated once in a shift by vacuum conveying system connected with the Electrostatic seperator hopper vacuum conveying system.

1.3.4 Dry Fly Ash Handling System

Fly ash is considered to be collected in electrostatic separator hoppers. Fly ash from electrostatic separator hoppers extracted by vacuum pumps transported to intermediate surge hopper cum bag filter for further dry Conveying to fly ash silo. Under each surge hopper ash vessels shall be connected with Oil free screw compressor for conveying the fly ash from Intermediate Surge Hopper to silo. Total fly ash generated from each unit will be conveyed through streams operating simultaneously and in parallel.

1.3.5 Ash Slurry Disposal System

Bottom Ash slurry, Fly ash slurry and the Coarse Ash slurry shall be pumped from the common ash slurry sump up to the dyke area which is located at a distance from Slurry pump house.

1.4 DIFFERENT TYPES OF LOSSES IN PIPELINES

When fluid flows through a pipe, it is subjected to hydraulic resistances which are of two types (i) Viscous frictional resistance (ii) Local resistance. Viscous frictional resistance associated with the fluid flow is called major loss of energy, where as local resistances are called losses of energy. Local resistances are essentially due to change of velocity either in magnitude or direction, in which the portion of energy possessed by the flowing fluid gets dissipated as heat energy. Losses due to change in cross section, bends, valves and frictions of all types are categorized as minor losses. In short pipes ,minor losses sometimes be more than the frictional losses. Losses due to the local disturbances of the flow in the conduits such as changes in cross-section, projecting gaskets, elbows, valves and similar items are called minor losses. So, minor losses can be defined as the losses that occur in pipelines due to bends, elbows, joints, valves, etc. In case of a very long pipe, these losses are usually insignificant in comparison to the fluid friction in the length considered.

Losses in horizontal pipeline

In horizontal pipe when $Z_1 = Z_2$ and diameter of pipe is constant; $V_1 = V_2$, hydraulic loss is equal to the head of pressure drop or head loss

$$h_l = (P_1 - P_2)/\rho g \qquad (1.1)$$

where, h_l = head loss (m)

Z_1 = Datum head at point 1(m)

Z_2 = Datum head at point 2(m)

P_1(pascals) and P_2 (pascals) are the pressures at point 1 and 2.

ρ = Density of the fluid.(kg/m^3)

g = Acceleration due to gravity(m/s^2)

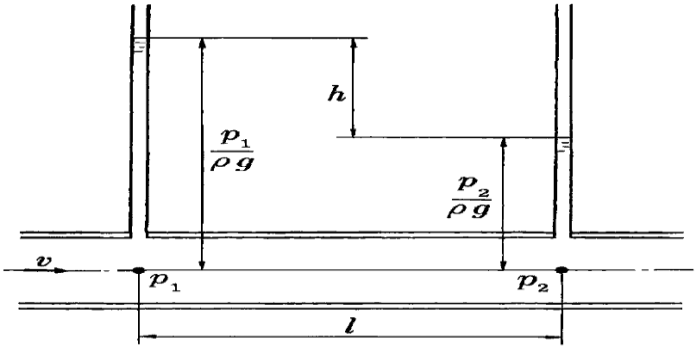

Fig 1.3: Pressure drop in horizontal pipe.

Head loss is expressed by Darcy -Weisbach equation:

$$h_l = \frac{FlV^2}{2gd} \tag{1.2}$$

Where ,

h_l = head loss due to friction(m)

l = Length (m)
V = velocity (m/s)
g = acceleration due to gravity (m/s^2)
d = diameter of pipe (m)
F = friction factor

1.4.1 Losses due to sudden contraction:

In the case of sudden contraction, the streamlines cannot follow the abrupt change of geometry and hence gradually converge from an upstream section of the larger tube. However, immediately downstream of the junction of area contraction, the cross sectional area of the stream tube becomes the minimum and less than that of the smaller pipe. This section of the stream is known as vena – contracta, after which the stream widens again to fill the pipe. In the deaccelerating part of the flow from Sec. c-c to Sec. 2-2 shown in Fig 1.4, where the stream tube expands to fill the pipe, losses take place .

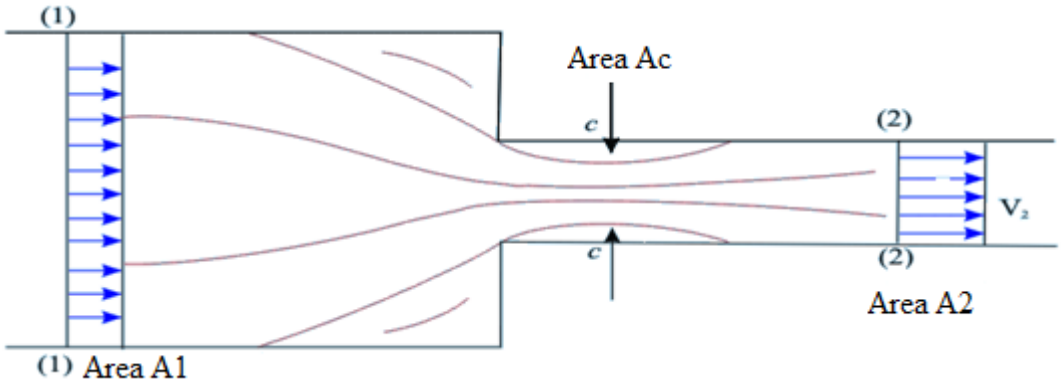

Fig 1.4: Pressure drop in sudden contraction

We can say that the losses due to contraction is not for the contraction itself, but due to the expansion followed by the contraction.

The loss of head in this case can be written as

$$h_l = \frac{V_2^2}{2g}\left[\left(\frac{A_2}{A_c}\right) - 1\right]^2 = \frac{V_2^2}{2g}\left[\left(\frac{1}{C_c}\right) - 1\right]^2 \tag{1.3}$$

Where,

h_l = head loss due to contraction (m)

V_2 = Velocity at section 2-2 (m/s)

V_1 = Velocity at section 1-1 (m/s)

A_2 = Area of section 1-1 (m^2)

A_c = Area at section c-c (m^2)

C_c = coefficient of contraction

$$C_c = \frac{A_c}{A_2} \tag{1.4}$$

Equation (1.3) is usually expressed as:

$$h_l = k\frac{v_2^2}{2g} \tag{1.5}$$

where, $$k = \left[\left(\frac{1}{C_c}\right) - 1\right]^2 \tag{1.6}$$

1.4.2 Losses due gradual contraction

Losses are given by:

$$h_l = \frac{kV_2^2}{2g} \tag{1.7}$$

Where, h_l =Head losses due to gradual contraction(m)

V_2 = Velocity at diameter D_1.(m/s)

k = loss factor

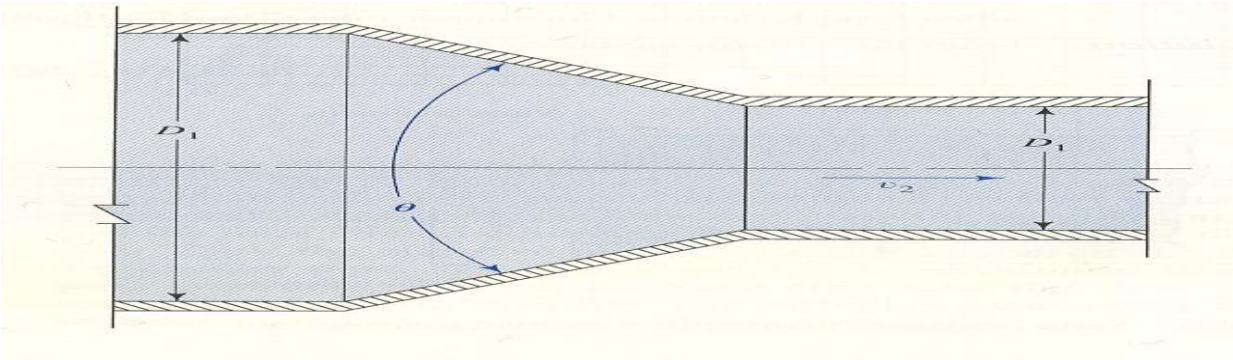

Fig 1.5: Pressure drop in gradual contraction

1.4.3 Losses due to gradual expansion

Losses are given by:

$$h_l = kV_2^2/2g \tag{1.8}$$

Where, h_l = Head loss due to gradual contraction(m)

V_2 = velocity at diameter D_2 (m/s)

g = Acceleration due to gravity (m/s^2)

k = loss factor

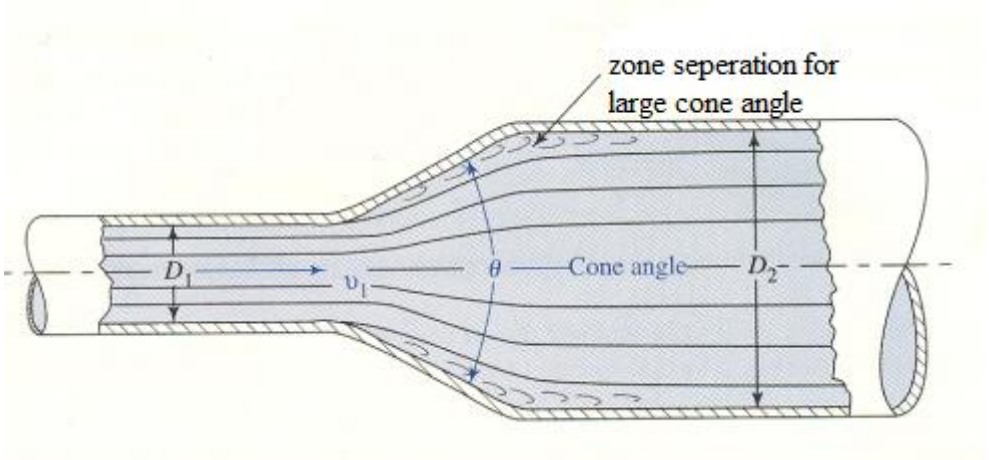

Fig 1.6: Pressure drop in gradual expansion

Loss in gradual expansion depends on the ratio of the pipe diameters and the angle of enlargement.

1.4.4 Losses due to sudden expansion

If the cross-section of a pipe with fluid flowing through it, is abruptly enlarged (Fig.1.7) at certain place, fluid emerging from the smaller pipe is unable to follow the abrupt deviation of the

boundary. The streamline takes a typical diverging pattern (shown in Fig.1.7). This creates pockets of turbulent eddies in the corners resulting in the dissipation of mechanical energy into intermolecular energy.

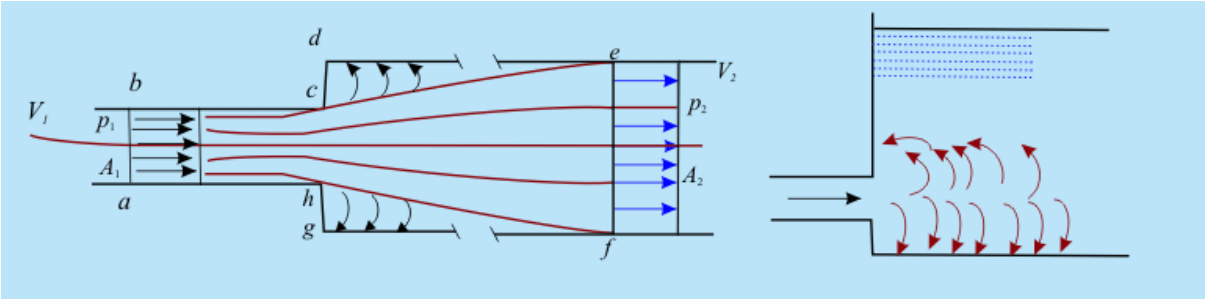

Fig 1.7: Head losses in sudden expansion

The fluid particles near the wall due to their low kinetic energy cannot overcome the adverse pressure hill in the direction of flow and hence follow up the reverse path under the favourable pressure gradient (from p_2 to p_1). This creates a zone of recirculating flow with turbulent eddies near the wall of the larger tube at the abrupt change of cross-section, as shown in Fig. 1.7, resulting in a loss of total mechanical energy. Due to the vigorous mixing caused by the turbulence, the velocity becomes again uniform at a far downstream section e-f from the enlargement (approximately 8 times the larger diameter).Hence, losses are given by:

$$h_l = \frac{(V_1 - V_2)^2}{2g} = \frac{V_1^2}{2g}\left[1 - \frac{A_1}{A_2}\right] \qquad (1.9)$$

Where h_l = Head loss due to sudden expansion (m)

V_1 = Velocity at section a-b (m/s)

V_2 = Velocity at section e-f (m/s)

A_1 = Area at section a-b (m^2)

A_2 = Area at section e-f (m^2)

g = acceleration due to gravity (m/s^2)

1.4.5 Losses due to bends

Bends are provided in pipes to change the direction of flow through it. An additional loss of head, apart from that due to fluid friction, takes place in the course of flow through pipe bend. The fluid takes a curved path while flowing through a pipe bend as shown in Fig. 1.8.

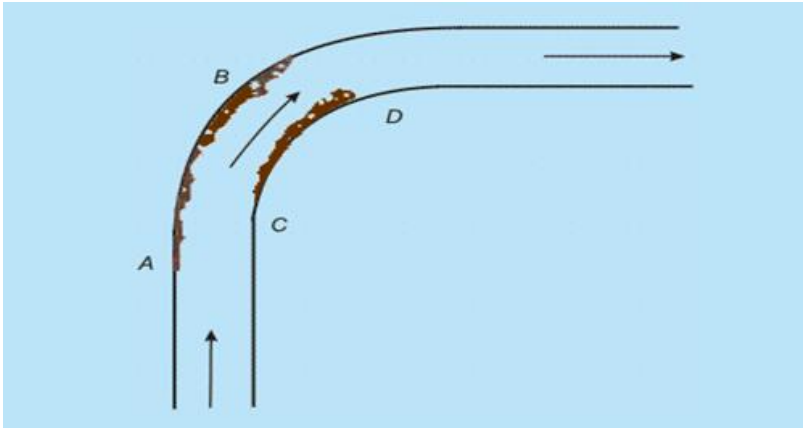

Fig 1.8: Losses in bend

Whenever a fluid flows in a curved path, there must be a force acting radially inwards on the fluid to provide the inward acceleration, known as centripetal acceleration . Fluid particles in this region, because of their close proximity to the wall, have low velocities and cannot overcome the adverse pressure gradient and this leads to a separation of flow from the boundary and consequent losses of energy in generating local eddies. Losses also take place due to a secondary flow in the radial plane of the pipe because of a change in pressure in the radial depth of the pipe**.**

The additional loss of head (apart from that due to usual friction) in flow through pipe bends is known as **bend loss** and is usually expressed as a fraction of the velocity head as

$$h_l = kV^2/2g \qquad (1.10)$$

h_l = Head loss due to bend (m)

V = Average velocity of the flow in bend (m/s)

g = Acceleration due to gravity(m/s^2)

k = loss factor

The value of *K* depends on the total length of the bend and the ratio of radius of curvature of the bend and pipe diameter *R/D*. The radius of curvature *R* is usually taken as the radius of curvature of the centre line of the bend. The factor *K* varies slightly with Reynolds number (Re) in the typical range of Re encountered in practice, but increases with surface roughness.

1.4.6 Entrance losses

Head losses at the entrance is given by

$$h_l = k\frac{V^2}{2g} \tag{1.11}$$

Where,

h_l = head loss duen to entrance (m)

V= velocity at the entrance (m/s)

g = Acceleration due to gravity (m/s^2)

k = loss factor

Different Values of k are shown in Fig 1.9(a),(b) and 1.9(c).

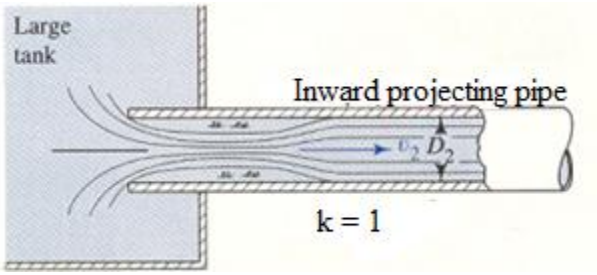

Fig 1.9(a): Head loss at entrance in case of inward projecting pipe.

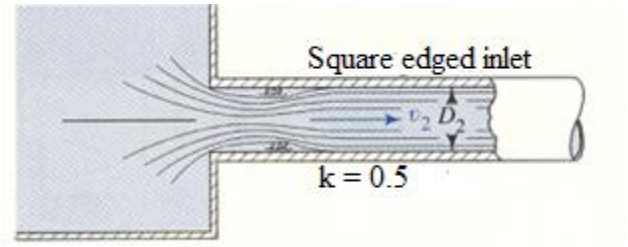

Fig 1.9(b): Head loss at entrance in case of square edged inlet

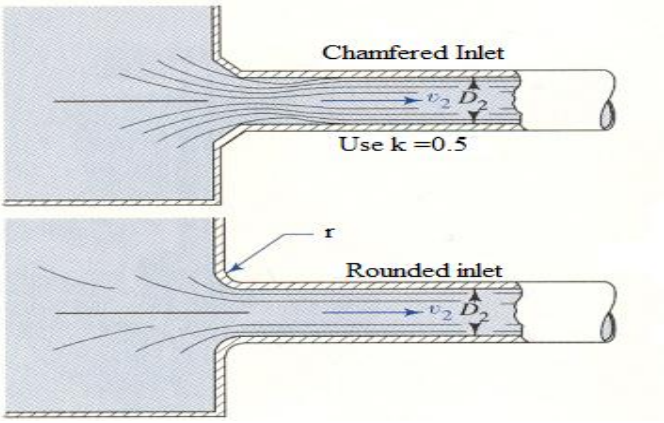

Fig 1.9(c) : Head losses at the entrance in case of chamfered and rounded inlet

1.4.6 Exit losses

This is the case where pipe enters a tank – a very large enlargement. The tank water is assumed to be stationery, that is, the velocity is zero. Therefore all kinetic energy in pipe is dissipated, value of K is 1.0. Fig 1.10 shows the head loss at the exit.

$$h_L = \left(\frac{V_1^2}{2g}\right) \tag{1.12}$$

Where,

h_L = Head loss at the entrance(m)

V_1 = Velocity at the exit of pipe.(m/s)

g = Acceleration due to gravity.(m/s^2)

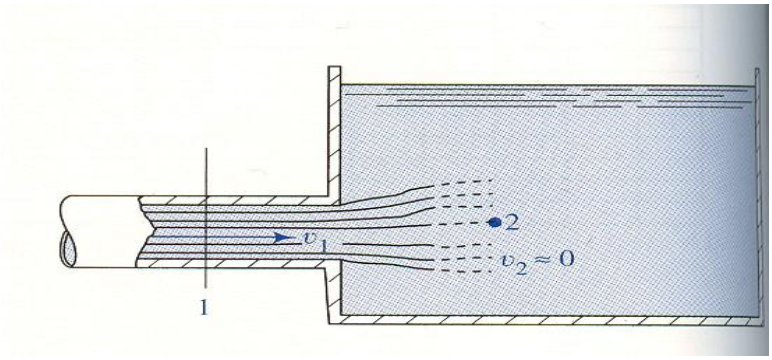

Fig 1.10: Head losses at the exit

CHAPTER 2
LITERATURE REVEIW

Transportation of materials comprising of very small particles such as pulverised coal and its ash through pipelines by mixing these with water or with some carrier fluid is proving a better option than conventional methods. This chapter gives an insight into the present state of knowledge about the flow characteristics in these pipelines by exploring the available literature.

2.1 PRESSURE DROP STUDIES IN SOLID LIQUID FLOW THROUGH PIPELINE

Mukhtar et al. (1995) studied the bend pressure drop on two materials, namely slurries of iron ore and zinc tailings. These two materials have been chosen because they differed widely in specific gravity as well as particle size distribution. From there experiments they observed that bend loss coefficient for long radius 90^0 bend in the flow of multi sized particulate slurry is less than that of water. Their study reveals that bend loss coefficient relatively independent of solid concentration and specific gravity. From their experiments they came to the conclusion that as long as the mixture velocity exceeds the deposition velocity by at least 0.5 m/s, the value of bend coefficient can be assumed to be independent of flow velocities.

Schimidt et al. (1997) investigated the pressure drop in the two-phase flow drop across a sudden contraction in a duct area and checked against data obtained with mixtures of air and water, aqueous glycerol, watery calcium nitrate and with the freon12.Experiments are performed for a wide range of conditions, pipe diameters and physical properties typically encountered in industrial piping systems. Based on the calculation, they concluded that unlike single phase flow two phase flow does not contract behind the edge of the transition at least in the range of mass flow quality in the range of 1% to 97%.They came on to the result that the contraction coefficient seems at least in two phase flow not to be physically reasonable parameter and should therefore not to be used as intermediate parameter to calculate the two phase pressure drop.

Gupta et al. (1997) investigated the flow of heterogeneous slurry around a horizontal bend and noticed the migration of larger particles towards the outer wall of the bend due to centrifugal forces. They concluded that bends also effect the drop size distribution of entrained drops in annular flow.

Rebeiro et al. (2000) investigated the drop size for air water horizontal annular flow for different gas and liquid flow rates and the effect of 90^0 horizontal bend on the drop size distribution. Characteristics of air water annular flow characteristics were established over a distance of 5m before encountering a 90^0 horizontal bend having radius of curvature of 0.166m.The pressure in the test section is maintained at 1.3 bar. After experiments they concluded that the gas velocity had a

strong effect on drop size because mean particle diameter is proportional to (superficial gas velocity)$V^{-1.}$ Drop size increases when flows through 90^0 horizontal bend.

Kaushal et al. (2002) measured the concenration profiles for six particle sizes ranging from 38 to 739 μm for multi sized particulate zinc tailings slurry flowing through 105 mm diameter horizontal pipe. They conducted the experiments at three flow velocities of 2, 2.75 and 3.5 m/s using five efflux concentrations ranging from 4% to 26% by volume for each velocity. Solids concentration varied with the vertical position, except for particle size of 38l μm. Experimental data for pressure drop were also collected at five efflux concentrations ranging from 4% to 26% at flow velocities ranging from 1.2 to 4.0 m/s for each efflux concentration.

Binding et al. (2006) performed numerical simulation and predicted the pressure field associated fluid through 4:1 contractions, 1:4 expansions and combined 4:1:4 contraction/expansions. Author studied the effect of the ratio of solvent to total viscosity parameter on the profile of the pressure gradient and on the entry and exit development lengths. From their investigation they concluded that flow through a contraction followed by an expansion, the pressure gradient on the centre-line shifts downstream as the Reynolds number is increased and the peak value of the pressure gradient decreases. Their experimental results revealed that the exit length for the used geometry increases significantly with reynolds number, for planar flow, but not in the case of axi-symmetric flow.

Fester et al. (2006) measured the pressure drop in three sudden contractions was using a range of Newtonian and non-Newtonian fluids. They provided a detailed procedure for the analysis of the results including the use of a kinetic energy correction factor for yield pseudoplastic fluids. Their investigations proves that same loss coefficients can be used for both Newtonian and non-Newtonian fluids in laminar and turbulent flow, provided that the Reynolds number used properly accounts for the viscous properties of the fluid. Their work has extended the database of results available over a wider range of Reynolds numbers and with more fluid types and contraction ratios.

Wael et al. (2007) developed an analytical formulation for the pressure recovery of two-phase flow across a sudden expansion. Author has performed the experiments using air–oil two-phase flow to evaluate the relative contribution of the different terms to the pressure recovery for three area ratios of 0.0625, 0.25 and 0.444. Experiments performed reveals that once the flow is fully developed downstream of the expansion, it has no memory of its formation. However, the flow in the developing region and the developing length are dependent on the upstream flow pattern and the area ratio.

At a very low mass quality, author observed that the pressure difference between the upstream flow and the downstream face of the expansion was very small. Increase in difference was observed when the upstream flow pattern was annular. Author observed that the contribution of the wall

pressure on the downstream face of the expansion is more significant than the additional viscous shear stress when the upstream flow is annular.

Chen et al. (2009) investigated the pressure change and flow pattern subject to the influence of sudden contractions. In their experiment the air and water mixture flows from small rectangular channels (2 × 4, 2 × 6, 4 × 4 and 4 × 6 mm, respectively) into a 2 mm diameter tube. The total mass flux ranges from 100 to 700 kg/m^2s with gas quality being varied from 0.001 to 0.8. In general the contraction pressure change increases with the rise of mass flux, and gas quality but an unique deflection of contraction pressure change pertaining to liquid vena contracta at a very low gas quality is encountered at a very low gas quality in the 4 ± 6 mm test section. Experiments performed by the author reveals that contraction pressure change generally increases with the gas quality, yet a special deflection of contraction pressure drop vs. gas quality is seen at a very low gas quality in the 4 × 6 mm test section. Author has also shown that elongated bubble becomes the dominate flow pattern when gas quality or the mass flux is small. However, the size of the elongated bubbles is detectably reduced when the aspect ratio is increased.

Liu et al. (2009) investigated the local resistance characteristics of coal–water slurry flowing through three types of piping components, namely gradual contractions, sudden contractions and 90^0 horizontal bends, at a transportation test facility. Author came on to the result that coal water slurry exhibits different rheological behaviours, i.e., the shear-thinning, Newtonian, and shear-thicken, at different shear rates. Author observed that when cola water slurry flows through the gradual contractions, the local pressure loss firstly decreases to a minimum, and then increases as the gradual contraction angle increases. From the experiments performed by the authors they concluded that when the coal water flow through the sudden contractions, with the increase of pipe diameter ratio, the local pressure loss increases for the two kinds of coal water slurry, whose mass concentration range from 57% to 59% and 59% to 62%, respectively as Reynolds number increases, local resistance coefficients of the three fittings declines quickly at first. However, with further increase in Reynolds number, local resistance coefficients shows different behaviours for the three fittings due to the special rheological property of coal water slurry at higher shear rates.

Senapati et al. (2009) investigated the rheological behaviour of five fly ash samples (having different mean diameter) collected from a thermal power plant over a range of volumetric solids concentration (ϕ=0.32–0.4945) in shear rate range of 10–200 s^{-1}.Author suggested that the slurry was highly pseudo-plastic whose behaviour can be described by a non-Newtonian power law model in the range of solids concentration studied. Author has determined the maximum solids fraction at which the slurry viscosity approaches infinity, for the fly ash samples using the relationship between inverse of relative viscosity and volume fraction of solids .

Balakhrisna et al. (2010) studied the change of flow patterns during the simultaneous flow of high viscous oil and water through the sudden contraction and expansion in a horizontal conduit. Author observed that these sudden changes in cross-section have a significant influence on the downstream phase distribution of lube oil–water flow. Author observed the pressure profiles during the simultaneous flow of lube oil and water through the sudden contraction and also compared with low viscous oil–water flows. This study reveals that an abrupt area change influences the phase distribution during oil–water flow through a horizontal pipe. Author concluded that the influence is more pronounced for lube oil–water as compared to kerosene–water flow. The flow patterns are influenced by oil properties. While viscous oils have a tendency to form different types of core annular flow, lighter oils exhibit a wider variety of distribution in water.

Mika (2011) has conducted the experimental studies using a few of the most common contractions of copper pipe sand presented the results of the experimental research on the ice slurry loss coefficient during its flow through sudden contractions. In his study he has covered six contraction ratios: 0.500, 0.615, 0.650, 0.769, 0.800 and 0.813. Author has performed the experiments varying the mass fraction of solid particles in the slurry ranged from 20 to 30 (20%, 25%, 30%). From the results author has developed the theoretical correlation for the ice slurry, in order to calculate the loss coefficient in contractions during laminar flow. The results of experimental investigations also confirmed that the loss coefficients in contractions in turbulent (transitional) flow of the ice slurry are the same as in the case of Newtonian liquids.

2.2 RHEOLOGICAL STUDIES ON COAL WATER AND COAL ASH WATER SLURRIES

Roh et al. (1994) investigated the factors affecting the rheological characteristics of coal-water mixture , including the properties of the coal, the volume fraction of solids and the mean size and size distribution of the coal particles. They measured the apparent viscosity with a Brookfield viscometer, and the non-Newtonian properties based on the power-law model were investigated using a Haake rotational viscometer at shear rates up to 512 1/s . Their results showed that the slurry exhibited shear thinning, i.e. pseudoplastic behaviour, and that it became more viscous as the mean particle size decreased, but less viscous with decreasing equilibrium moisture content. Author reveals that the degree of pseudoplasticity increased with increasing coal content and with decreasing mean size of particles. Experiments performed by the author reveals that the mixing of coarse and fine coal particles was found to be very effective in obtaining mixtures characterized by high solids content and low viscosity. Author also concluded that coal water mixture viscosity was lowest when the blending ratio of fines was 0.35, irrespective of the mean-size ratio

Logos et al. (1996) studied the rheological behaviour of a low-rank coal-water slurry from Lochiel, South Australia, as a function of solids concentration, particle size and size distribution. They found that coal slurries consisting of particles finer than 45 μm suspended in water exhibit a wide spectrum of flow behaviour ranging from Newtonian at low solids concentrations to shear-thinning. After performing the experiments author observed that rheological properties of a South Australian coal-water slurry can be improved simply by modifying the size distribution of the coal particles. Addition of a coarser coal fraction to a suspension of fine coal solids can substantially lower the viscosity of the resulting bimodal coal slurry. Author found out the optimum ratio of coarse-to-fine particles at which the slurry viscosity is at minimum. Author also reveals that on adding more coarse particles at proportions greater than the optimum composition does not significantly affect the rheological properties but may cause destabilization of the slurry. Author concluded that, it is possible to reduce the slurry viscosity further by blending more than two different size fractions and by carefully controlling the composition of the different fractions.

Iyer et al. (2000) investigated that when the flow of dense slurries of fine particles of fly ash is characterised, it is convenient to define a new packing fraction , which includes the volume of the double layer. The diffuse double layer thickness, which is a function of the ionic strength, leading to an increase in maximum packing fraction . Author predicted the increase in (maximum packing fraction) that is found from experimental flow data at low shear rates.

Turian et al. (2002) investigated the properties, settling rates, and the rheology of coal–water mixtures made up from different coals. Author made up the test suspensions containing different concentrations of suspended particles from each of four different pulverized parent coals. Experiments performed by the author reveals that, highly loaded coal water mixture exhibit strong non-Newtonian behaviour, which is further reinforced when the concentration of suspended solids increased. They found that the behaviour of concentrated suspensions made up of coarser suspended particles with a narrow particle-size distribution is Newtonian. They concluded that the viscosities of the suspensions are markedly increased as the concentration is increased. Author also concluded that the rheological behaviour of suspensions made up of fine particulate coal having a broad size distribution is non-Newtonian; and exhibiting shear-thinning.

Boylu et al. (2003) determined the chemical and physical properties of the coal samples, their zeta potentials. To determine the effect of volume fraction on the viscosity of the slurry, the pulps of different solids percentage composed of coal particles with mean diameter sizes of 19, 35 and 50 μm were used. They found that the effect of particle size distribution and density on the viscosity was in good agreement with the findings of other investigators. Author investigated the effect of volume fraction venation on the viscosity for heterogeneous and homogeneous mixtures prepared with different ranks of coals. It was also observed that the viscosity increases with increasing pulp

density by weight for various particle size distributions. The results can be explained on the basis of the fact that coals of different ranks exhibit different chemical and physical properties such as porosity, specific surface areas, etc.

Yuchi et al. (2007) investigated the effects of coal characteristics on the properties of coal water slurry using sixteen Chinese coals of different ranks from lignite to anthracite. From his investigation author concluded that the carbon content and grindability index of coal showed a positive correlation with the slurry ability. Experiments performed by the author reveals the rheological behaviour of CWS can be positively correlated with ash content, content of soluble ions, while zeta potential properties of the coal surface negatively impact the rheological behaviour.

Senapati et al. (2010) investigated shear thinning behaviour for different fly ash samples at higher solids volume fractions in the range 0.32–0.49. Their study indicated that the relative viscosity is very much sensitive to the concentration of solids, particle size and particle size distribution. After investigations, author concluded that the laminar flow regime can be identified after determining the transition Reynolds number for each specific fly ash samples in specified range of shear rates and solids concentration.

Zengjie et al. (2011) studied the effect of ash content and particle size gradation on rheological properties. Author selected two coals with different grinding times and particle size analysis. Author measured the concentration, viscosity, fluidity, and stability of each coal water slurry sample. From their investigations author concluded that found that the ash content of Australian coal is 21.72% higher than the ash content of Chinese coal. Author concluded that the fluidity and stability of the coal water slurry prepared from the Australian coal are both better than the fluidity and stability of slurry prepared from Chinese coal.

Bentz et al. (2012) investigated the influence of three variables (cement particle size distribution , fly ash particle size distribution, and ratio of fly ash to cement) at each of four levels on the yield stress and viscosity of blended paste. From the experiments author concluded that both particle densities and particle surface areas, determined from measured particle size distributions, are critical parameters that influences rheological properties. Their investigations reveals that yield stress is dominated by the particle density of the cement component, fly ash mainly acting as a diluent that effectively decreases the cement particle number density. Author also concluded that viscosities are influenced by both cement and fly ash particles, with approximate linear relationships between plastic viscosity values and either total particle surface area or total particle density being found.

2.3 COMPUTATIONAL STUDIES IN SOLID LIQUID FLOW THROUGH PIPELINE

Sowjanya et al. (2005) used the commercially available Computational Fluid Dynamics code to simulate the complex flows in the piping systems in a power plant. They employed the two-phase modelling technique for the estimation of the pressure drop coefficients with both clean air and coal/air flows in order to size the orifices. They concluded that the pressure drop in the systems strongly depends on the system geometry. From their numerical investigations, they provided detailed information of the two-phase flow field in the piping systems in a power plant, based on which physical insights were obtained and better understanding of the complex flow phenomena was achieved. Their study demonstrated that computational fluid dynamics can be used as an effective tool for design and research for power industry applications.

Eesa & Barigou (2008) performed the numerical simulation on the horizontal flow of coarse particle suspensions in non-Newtonian carrier fluids using an Eulerian–Eulerian computational fluid dynamics model. They concluded that computational fluid dynamics is, capable of predicting the flow of homogeneous suspensions which can be approximated by single phase rheology such as pseudoplastic and viscoplastic types which are representative of many industrial suspensions. Simulation results showed that velocity profiles of particles near the top of the pipe cross-section moved significantly faster than particles at the bottom. Author also concluded that that the position of the maximum particle velocity was not at the pipe centreline but a few millimetres above it. The presence of solid particles resulted in a significant degree of a symmetry and flattening in the carrier fluid velocity profile, especially at high solids concentrations.

Margherita et al. (2010) used the computational fluid dynamics commercial code to evaluate the pressure drop through pipes in a stream of high pressure gas. Author considered both hexahedral and tetrahedral grids are considered. Preliminarily, a grid sensitivity analysis is carried out by comparing computational fluid dynamics results with analytical results. In order to investigate the behaviour of the grid with respect to the boundary layer each grid is characterized by a different number and thickness of layers. Author validated his by using a literature test case, in which high pressure gas flow through a rough pipe is experimentally studied. Simulation results showed that the radial depth of the prism layers on pipe wall has to be high enough to allow the correct resolution of the boundary layer. Author has carried out a grid sensitivity analysis out for rough pipes characterized by different roughness height in terms of equivalent sand grain. The analysis highlighted that the first element height of the prism layer should be high enough to avoid inconsistencies in the rough model application. Their investigations reveals that the grid used for calculations does not strongly influence the numerical results and hence the use of the hexahedrals and teterahedrals grid is not always justified. For low values of the equivalent sand grain roughness, numerical values of the friction factor are in good agreement with experimental data.

Pan Shi et al. (2010) developed a three-dimensional computational fluid dynamics, model, using a Eulerian–Eulerian two-fluid model, to describe the steady-state liquid–solid two-phase flow in test loop and axial flow pump. Author carried out the corresponding simulations in the commercial computational fluid dynamics code Fluent. Form the simulation results author concluded that the predicted pressure gradient data were found to agree well with the classical calculated data. The solid particles always aggregate at the outside of curve section because of the difference between the densities of the solid phase and the liquid phase. In addition, the turbulence leads to the uniform distribution of the solid phase in the straight pipe.

Kaushal et al. (2012) performed the numerical simulation of pipeline slurry flow of mono-dispersed fine particles at high concentration using Mixture and Eulerian two-phase models. Both the models are part of the Computational fluid dynamics, software package FLUENT. A hexagonal shape and cooper type non-uniform three-dimensional grid are chosen to discretize the entire computational domain. Author used a control volume finite difference method to solve the governing equations. Simulation results showed that mixture model fails to predict pressure drops correctly. The amount of error increases rapidly with the slurry concentration. Investigation of author reveals that Eulerian model gives fairly accurate predictions for pressure drop at all the efflux concentrations and flow velocities. The concentration distributions obtained using Eulerian model found to be in good agreement except for few experimental data near the pipe bottom. Author concluded that the lateral variation of solids concentration in the pipe cross-section is more dominant at higher concentrations and flow velocities. The higher concentration zone at higher velocities and concentrations is situated in the lower half portion of pipeline away from the surrounding pipe boundary.

CHAPTER 3

RHEOLOGICAL STUDIES ON BOTTOM AND FLY ASH MIXTURES

Rheology characteristics of slurry depend up on various factors such as particle size distribution, pH, settling characteristics, specific gravity etc. Change in these characteristics of slurry shows a significant change in the viscosity of the slurry. Therefore, analysis of mentioned factors is to be done for given sample. In present study particle size distribution, pH, settling characteristics, specific gravity are found for the bottom and fly ash samples.

3.1.1 Particle Size Distribution

The particle size distribution of a material can be important in understanding its physical and chemical properties. The way particle size distribution is usually defined by the method by which it is determined. The most easily understood method of determination is sieve analysis, where particles are separated on sieves of different sizes. Thus, the particle size distribution is defined in terms of discrete size ranges: e.g. "% of sample between 45 μm and 53 μm", when sieves of these sizes are used. The particle size distribution is usually determined over a list of size ranges that covers nearly all the sizes present in the sample. Some methods of determination allow much narrower size ranges to be defined than can be obtained by use of sieves, and are applicable to particle sizes outside the range available in sieves. However, the idea of the notional "sieve", that "retains" particles above a certain size, and "passes" particles below that size, is universally used in presenting particle size distribution data of all kinds.

3.1.2 Settling Characteristics

Settling is the process by which particulates settle to the bottom of a liquid and form a sediment. Particles that experience a force, either due to gravity or due to centrifugal motion will tend to move in a uniform manner in the direction exerted by that force. For gravity settling, the particles will tend to fall to the bottom of the vessel, forming a slurry at the vessel base. For settling particles, there are two main forces enacting upon any particle. The primary force is an applied force, such as gravity, and a drag force that is due to the motion of the particle through the fluid. The applied force is usually not affected by the particle's velocity, whereas the drag force is a function of the particle velocity. For a particle at rest no drag force will exhibited, which causes the particle to accelerate due to the applied force.

In present work settling analysis is performed for fly and bottom ash. Particles in the slurry gets settle down when it is kept at rest. For settling analysis a standard cylindrical flask has been used. Cylindrical flask has calibrated markings to measure the volume of solids accumulated in the bottom after settling in given time. In the present work, to determine the static settled concentration, a slurry sample of intermediate concentration i.e. 20% (by weight) is prepared and allowed to settle in a cylindrical flask till solids become constant at particular level. The value of solid concentration which gets settled down is the static settled concentration. At regular intervals of time the slurry level is also recorded to determine the settling rate of the slurry during the process of settling.

3.1.3 pH value

pH tells the nature if the sample is basic or acidic. In the present study pH value of ash samples are measured with the help of pH meter. A pH meter is an electronic instrument used for measuring the (acidity or alkalinity) of a liquid though special probes. A typical pH meter consists of a special measuring probe (a glass electrode) connected to an electronic meter that measures and displays the pH reading.

3.2 RHEOMETER

Variation of shear rate and shear stress of ash slurry is found out by ANTAN PAAR rheometer (shown in Fig3.1). Various mixtures of bottom and fly ash with different solid concentrations are tested on the rheometer. The slurry is placed within the annulus of one cylinder inside another. One of the cylinders is rotated at a set speed. This determines the shear rate inside the annulus. The slurry tends to drag the other cylinder round, and the force it exerts on that cylinder (torque) is measured, which can be converted to a shear stress. In the present study the shear stress value and viscosity measured at the shear rate range from 0-300 s^{-1} at the constant temperature condition 26 °C with wide range of concentrations varying from 20 to 50% (by weight) for ash and water slurries. Stress versus shear rate graphs are plotted with bottom ash and fly ash with different ratios.

Fig 3.1 Rheometer (Antan Paar)

3.3 PHYSICAL PROPERTIES OF BOTTOM AND FLY ASH

Physical properties of bottom ash and different mixture ratios are shown in figures below. The specific gravity of bottom ash was determined as 2.25. Energy-dispersive X-ray spectroscopy of fly and bottom ash is shown in Fig.3.2 and Fig 3.3. Zoomed pictures from scanning electron microscope of Fly and Bottom Ash are shown in Fig 3.4 and Fig 3.5 Particle size distribution of bottom ash and fly ash are shown in. Fig 3.7 shows the settling rate of bottom and fly ash. Figures 3.8(a),(b),(c),(d),(e) shows the variation of shear rate with shear stress at various concentration range (20% to 50%) of bottom and fly ash.

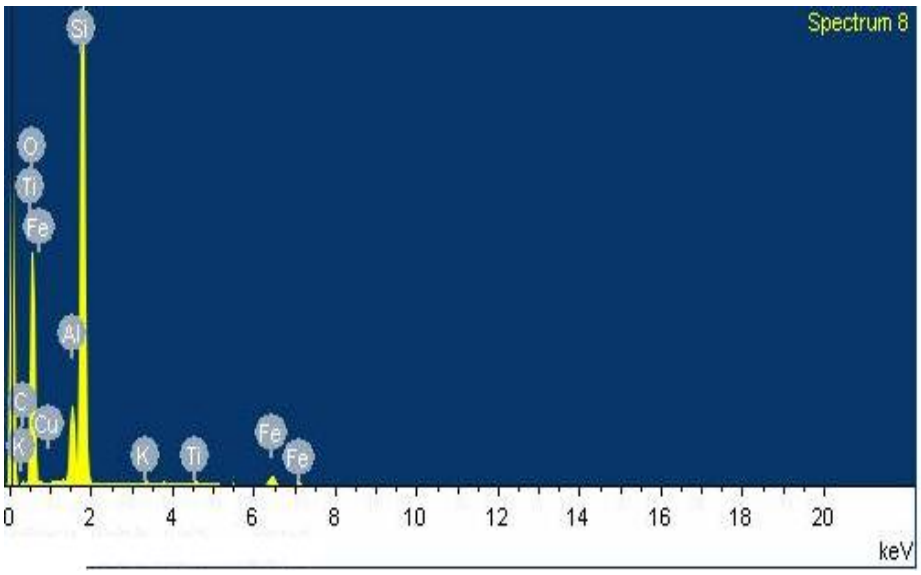

Fig: 3.2: Energy-dispersive X-ray spectroscopy of bottom ash

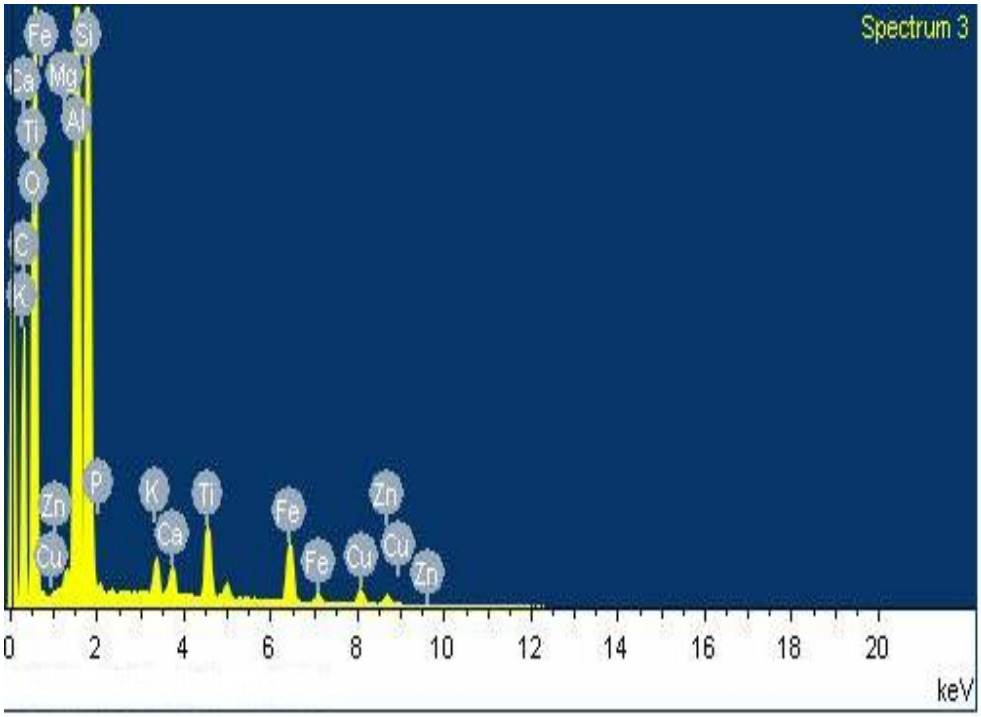

Fig 3.3: Energy-dispersive X-ray spectroscopy of fly ash

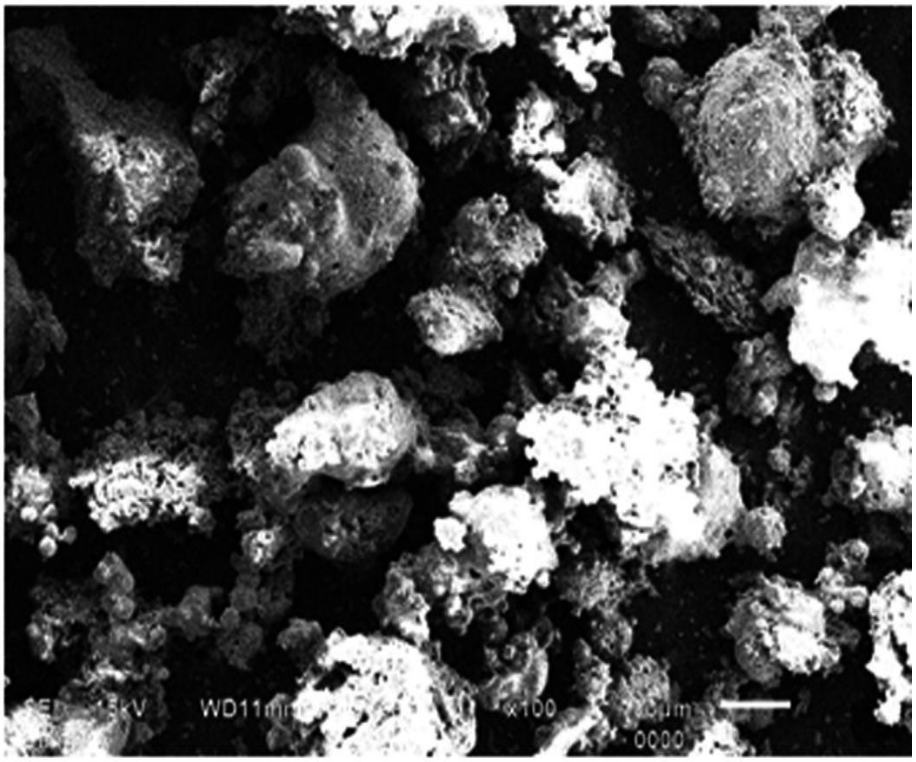

Fig 3.4: Scanning electron microscope picture of bottom ash.

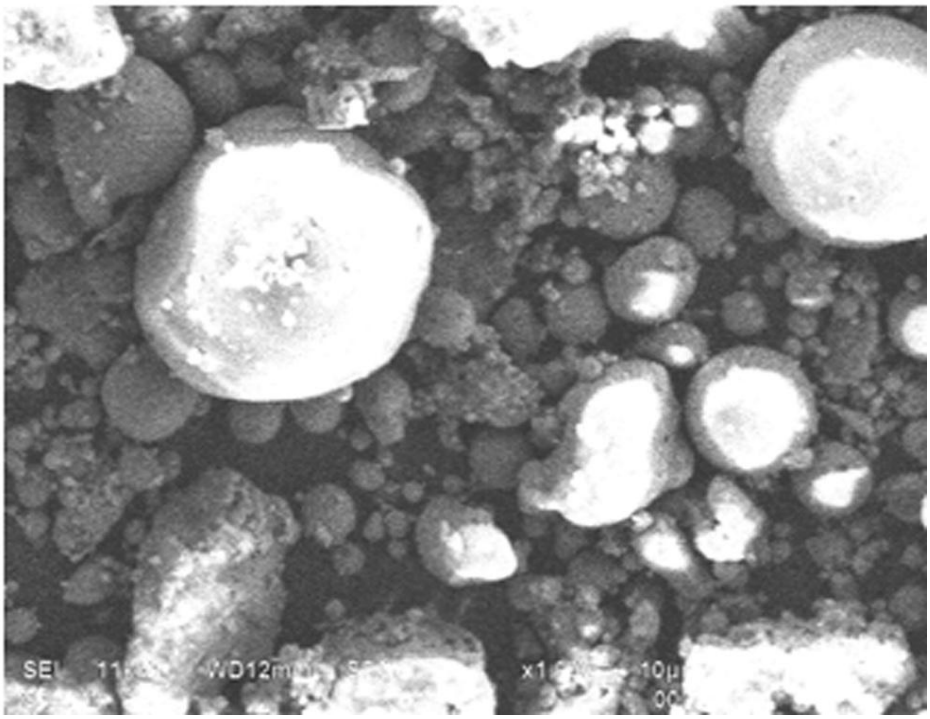

Fig 3.5: Scanning electron microscope picture of fly ash.

3.4 GRAPHICAL REPRESENTATION OF PROPERTIES OF BOTTOM AND FLY ASH

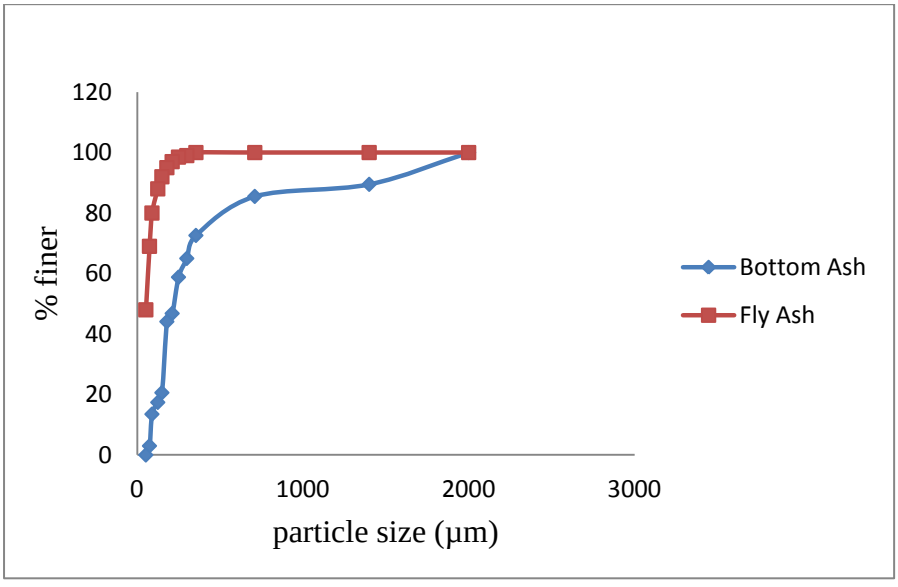

Fig: 3.6 Particle size distributions of bottom and fly ash.

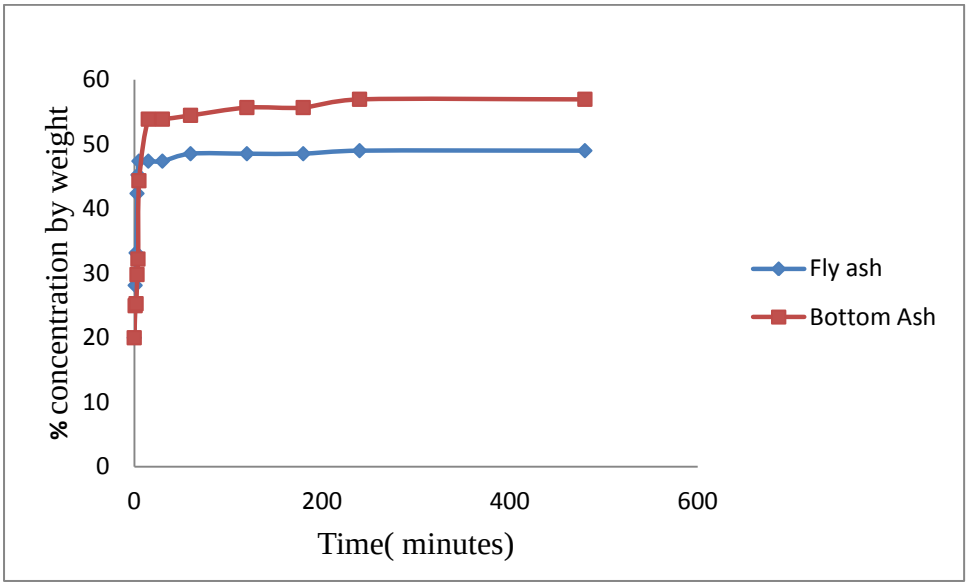

Fig 3.7: Settling characteristics of bottom and fly ash at 20% concentration by weight.

Fig 3.6 shows that the largest particle for bottom ash is 2000µm and only 3% particles are finer than 75µm. In case of fly ash all particles are finer than 355 µm and 48% particles are finer than 53µm. Fig 3.7 shows that 56.98% bottom ash and 49.01% fly ash sample has been settled in 480 minutes.

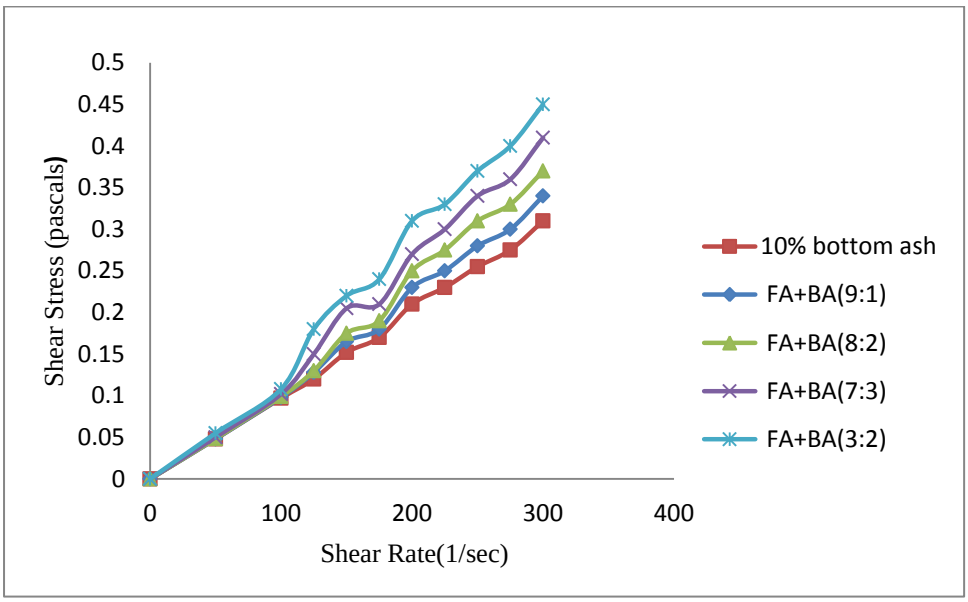

Fig 3.8(a): Shear stress - shear rate variation with 10% concentration by weight for different ratios of bottom and fly ash.

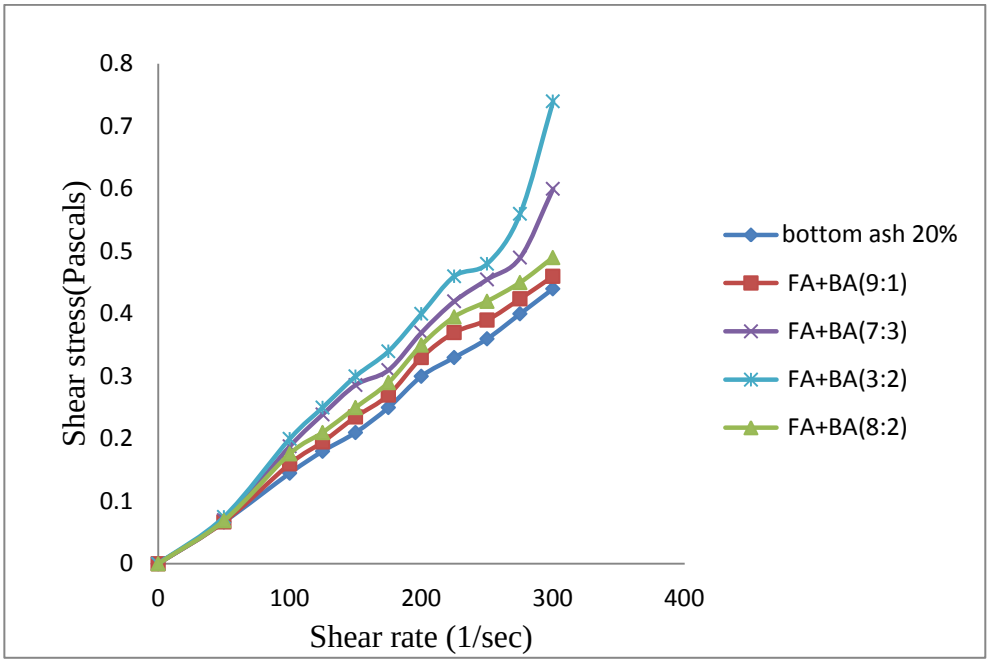

Fig 3.8(b): Shear stress versus shear rate variation with 20% concentration by weight for different ratios of bottom and fly ash.

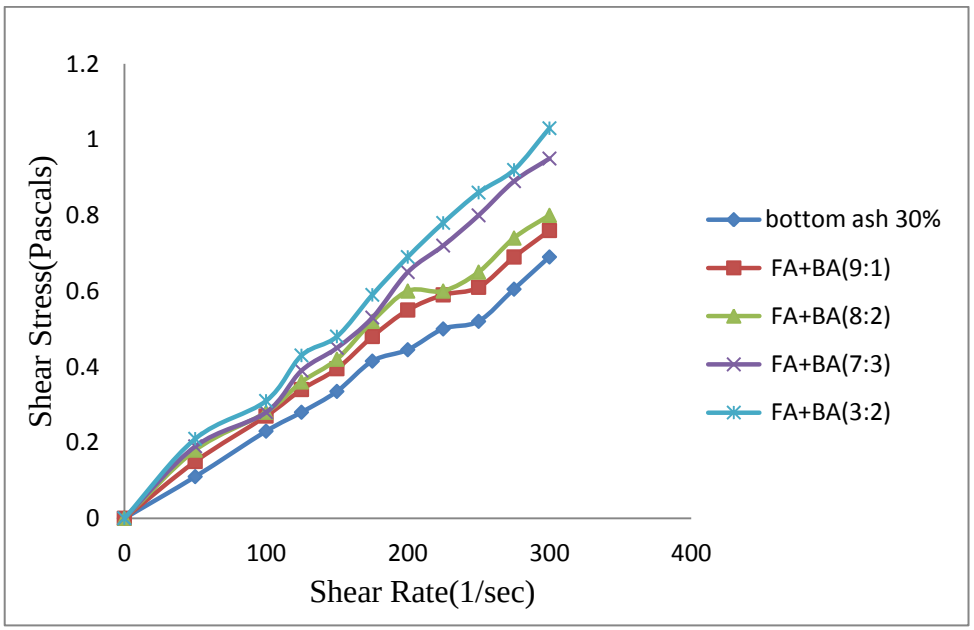

Fig 3.8(c): Shear stress versus shear rate variation with 30% concentration by weight for different ratios of bottom and fly ash.

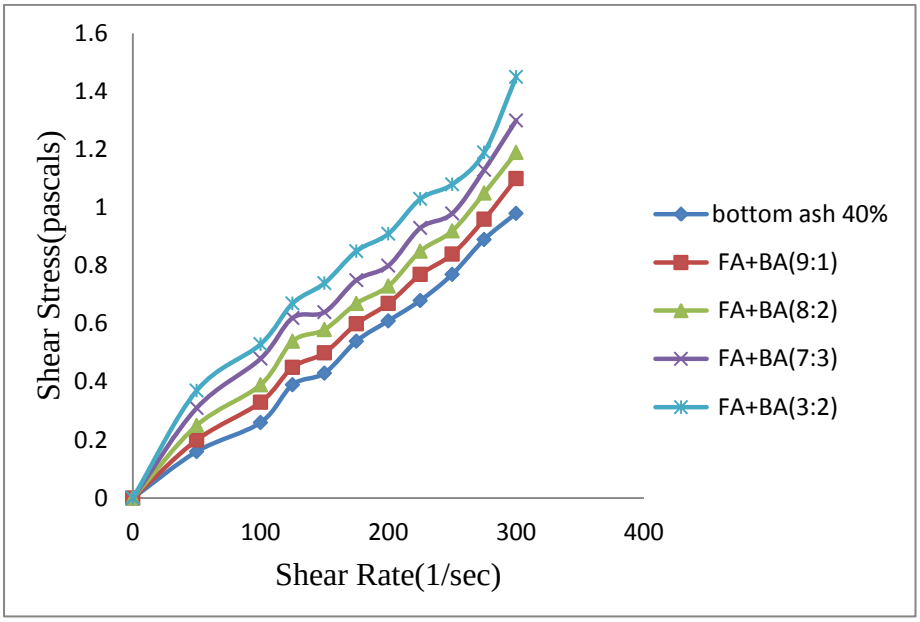

Fig 3.8(d): Shear stress versus shear rate variation with 40% concentration by weight for different ratios of bottom and fly ash.

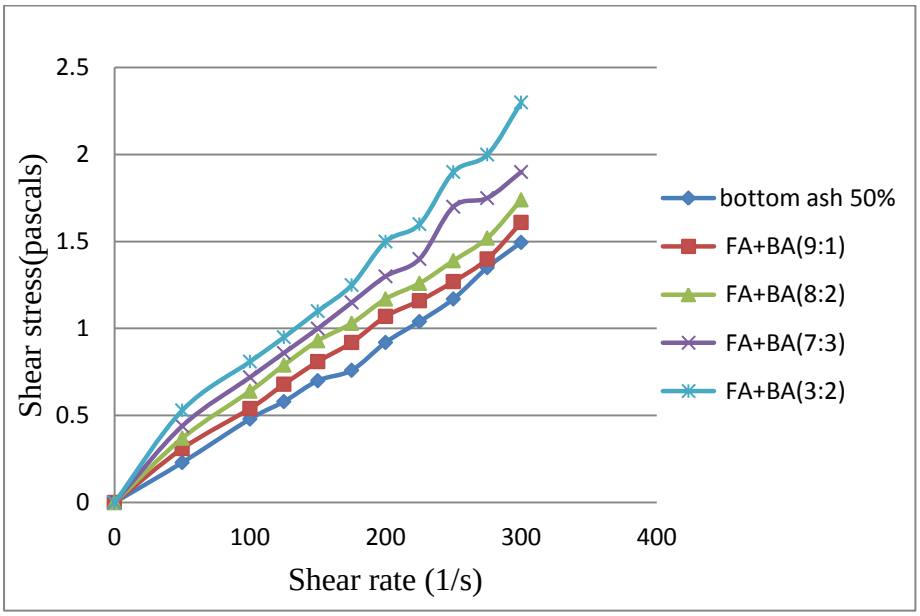

Fig 3.8(e): Shear stress versus shear rate variation with 50% concentration by weight for different ratios of bottom and fly.

Fig 3.8(a)-(e) shows that slurry almost behaves as Newtonian fluid at all solid concentration taken for evaluation. Relative increase of shear stress with shear rate for Bottom ash + Fly ash (3:2) is maximum and relative increase of shear stress with shear rate for bottom ash is minimum. As the percentage of bottom ash decreases in the mixture, relative rise in shear stress increases.

CHAPTER4

NUMERICAL EVALUATION OF PIPELINE

Computational fluid dynamics usually abbreviated as **CFD**, is a branch of fluid mechanics that uses numerical methods and algorithms to solve and analyze problems that involve fluid flows. CFD simulations are used to model fluid flows over a wide range of physical scales. The fundamental of the CFD simulation is the conservation of equations. Computers are used to perform the calculations required to simulate the interaction of liquids and gases with surfaces defined by boundary conditions.

4.1 METHODOLOGY

There are three main steps to solve a computational fluid dynamics problem.

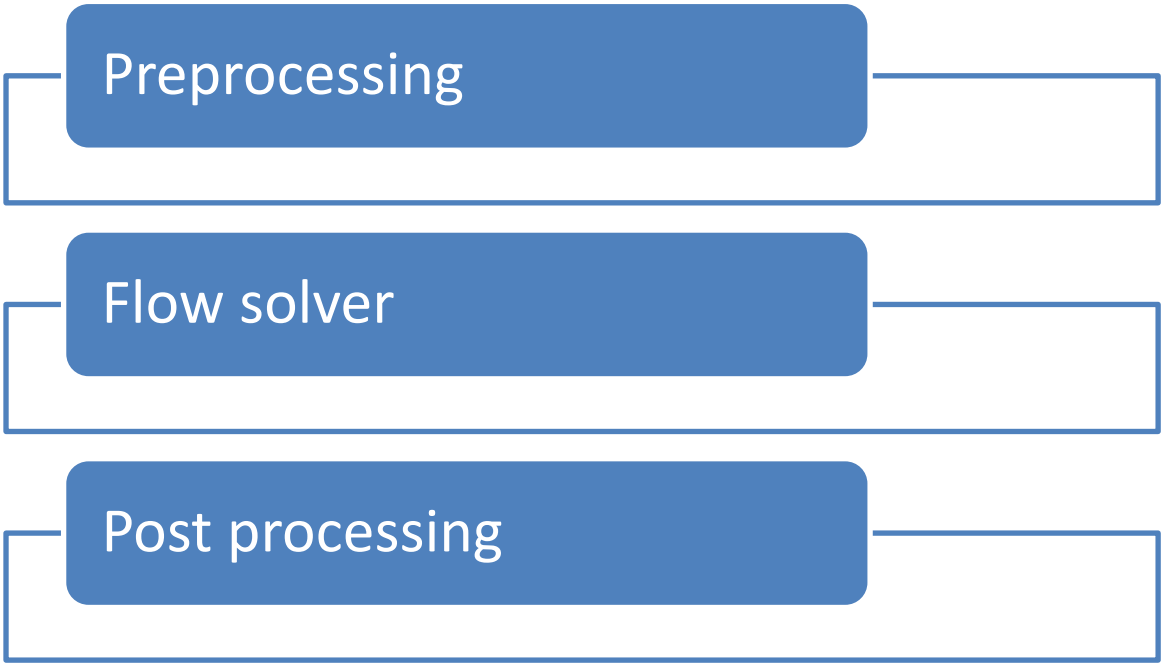

4.1.1 Preprocessing

First step in preprocessing is the definition of the geometry of the region of interest. Definition of geometry is followed by grid generation. Grid generation is the sub division of domain in the number of smaller sub domains e.g grid, cells, control volumes. After this appropriate boundry conditions are defined. Boundary condition involves the specification of the fluid behaviour and properties at the boundaries of the problem.

4.1.2 Flow Processor

In Flow solver the simulation is started and the equations are solved iteratively as a steady-state transient. There are mainly three methods for this solver.

(i) Finite volume method
(ii) Finite element method
(iii) Finite difference method

In the finite volume method governing equations are in the integral form. In this method the solution domain is subdivided into a finite number of contiguous control volumes. After this conservation equation is applied to each control volumes. Computational node locates at the centroid of each control volume. One of the advantage of this method is that it can be applied to any types of grids, especially complex.

Finite element method is similar to finite element method. In this method governing equations are multiplied by a weight function before integrated over the entire domain. The finite element method formulation requires special care to ensure a conservative solution. This method is more stable than the finite volume method.

Finite difference method uses the governing equations in differential form. In this method solution domain is subdivided in the grids. This method replaces the partial derivatives by approximations in terms of node values of the functions. One algebraic equation per grid node is present. Linear algebraic equation system is used in this method. Finite difference can be applied to structural grids.

4.1.3 Post processor

Finally a postprocessor is used for the analysis and visualization of the resulting solution It displays the domain geometry and grid. Vectors, contours plots are used to visualize the results.

4.2 MODELING OF STRAIGHT PIPE

For the study of numerical evaluation of pipeline, a straight pipe is modeled to study per unit length pressure drop. Modeling of straight pipe is done in Gambit software version 2.2. Three dimensional model of straight pipe is shown in Fig 4.1

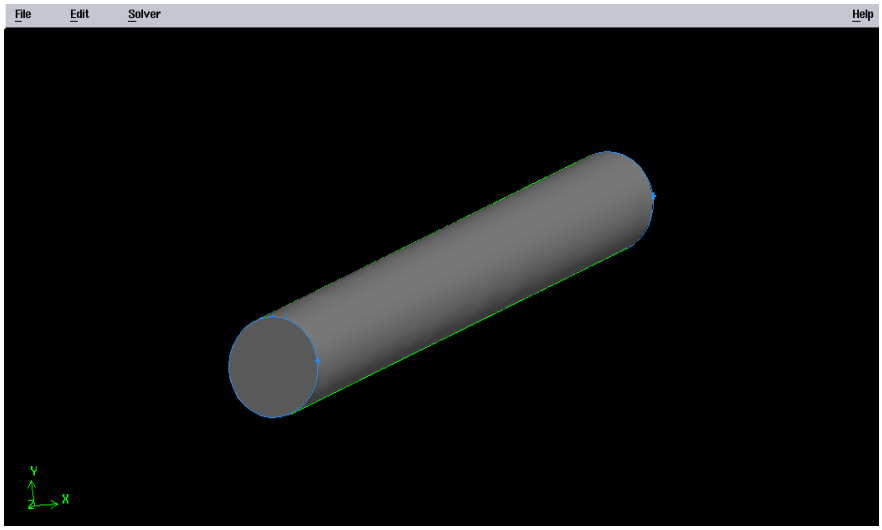

Fig. 4.1: Model of straight 1 metre pipe

4.2.1 Mesh examination

Mesh generation is a very important part in the numerical evaluation. It is very important to check the quality of generated mesh. Different meshes are generated in given models and mesh selection is based on various factors such as skewness and aspect ratio. There are two methods for determining skewness. First is based on the equilateral volume:

$$\text{Skewness} = \frac{\text{optical cell size} - \text{cell size}}{\text{optical cell size}} \tag{4.1}$$

This applies only to triangles and tetrahedral.Second is based on the deviation from a normalized equilateral angle:

$$\text{Skewness (for a quad)} = \max\left[\frac{\theta_{max}-90}{90}, \frac{90-\theta}{90}\right] \tag{4.2}$$

It is applied to all cell and face shapes .It is always used for prisms and pyramids.

4.2.2 Grid independency test :

Results of pressure drop for different types of mesh has been evaluated .Results are compared with value obtained by using analytical formula for pressure drop in straight pipe for water i.e

$$\frac{\nabla P}{L} = \frac{f\, v^2}{2gd} \tag{4.3}$$

Where ∇P = Pressure drop
L = Length
v = velocity
g = acceleration due to gravity

d = diameter of pipe

Where f = friction factor and is calculated as

$$f = \frac{0.3164}{R^{0.25}} \quad (4.4)$$

Where , R is Reynolds number.

Table 4.1 Comparison of the parameters of various meshes and % error for the pressure drop in the straight pipe.

Element type	Element size	Elements	Skewness	Aspect Ratio	% error
Hexahedral	4	56784	0.39	1.616	8.8
Mixed	4	151726	0.74	2.98	5.2
Tetrahedral	4	276033	0.74	2.98	8.7
Hexahedral	3	84405	0.39	1.81	9.4
Mixed	3	212062	0.74	2.98	9.2
Tetrahedral	3	290653	0.74	2.95	9.3

From the above table it is found that mixed meshing element type with size of 4 resulted minimum percentage of error in pressure drop per unit length. Therefore, mixed element type meshing with element size 4 has been used for simulation. Fig 4.2 shows the meshed straight pipe.

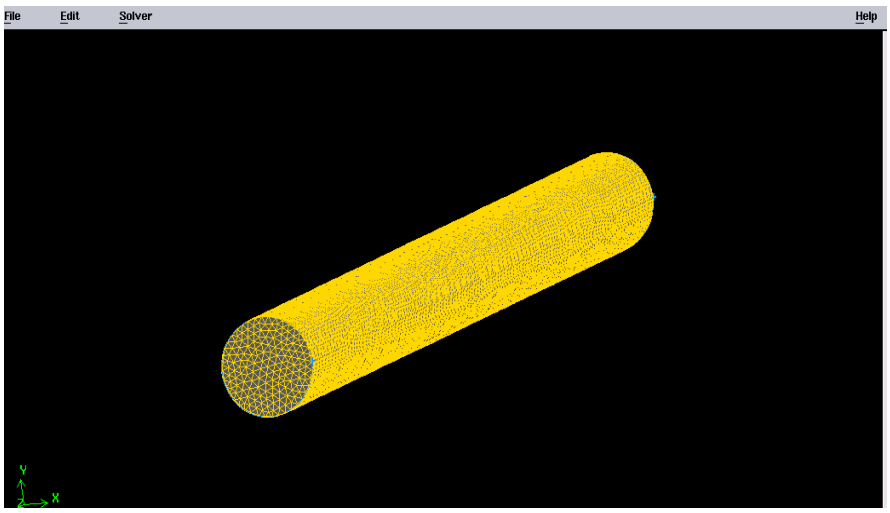

Fig 4.2: Meshed 1 metre straight pipe

4.3 ASSUMPTIONS FOR SIMULATION

Basic assumptions on which the simulation is done are as follows

1. Steady state condition
2. Incompressible fluid flow

3. Constant fluid properties

4.3.1 Boundary conditions

1. Constant inlet velocity is taken for particular simulation .

2. Pressure at the outlet is taken 0 or atmospheric gauge pressure.

3. 4 % turbulence intensity and turbulence viscosity ratio of 10 is taken for inlet condition

4. 4% backflow turbulence intensity and backflow turbulence viscosity ratio of 10 is taken for outlet condition.

4.3.2 Solution parameters

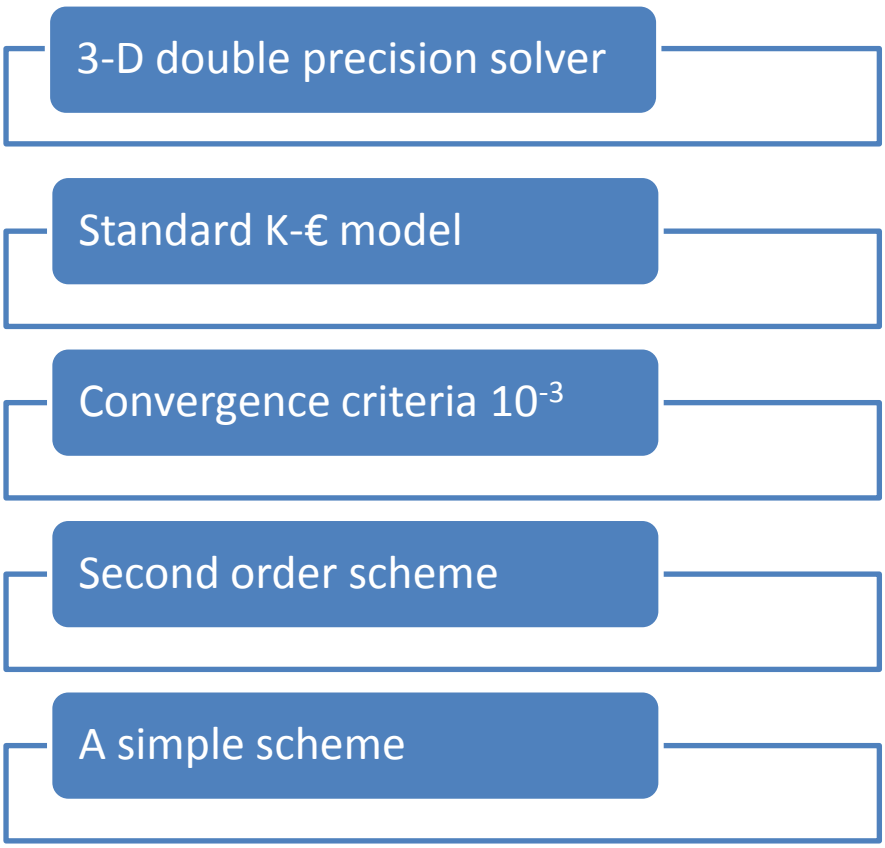

4.4 SIMULATION RESULTS OF STRAIGHT PIPE

Fig 4.3(a)-(d) shows the pressure variation in straight pipe at different bottom and fly ash mixture with different flow velocities from 1.5 to 3.

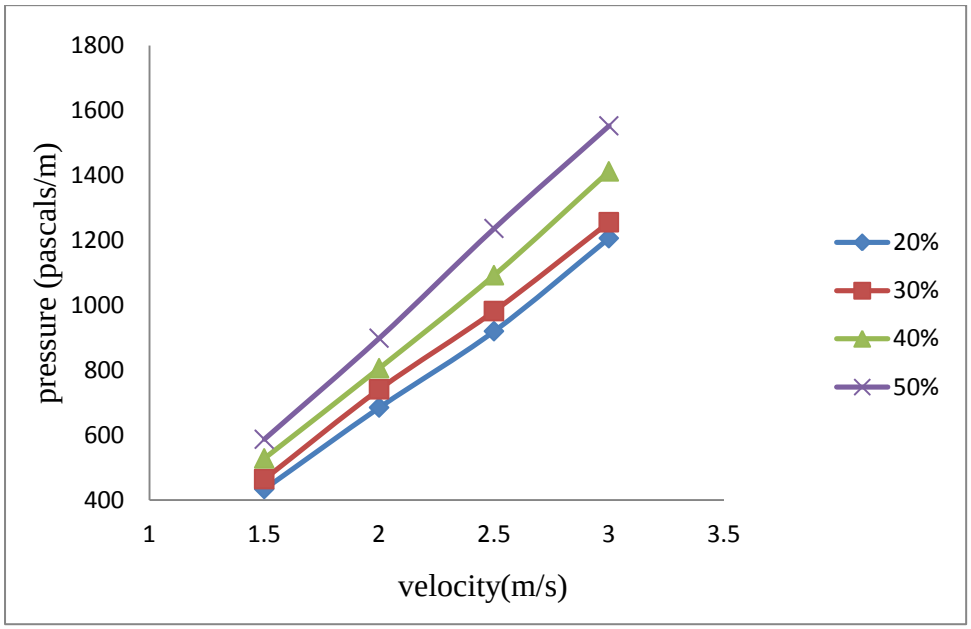

Fig 4.3(a): Pressure variation in straight pipe with 6:4 (B.A:F.A)

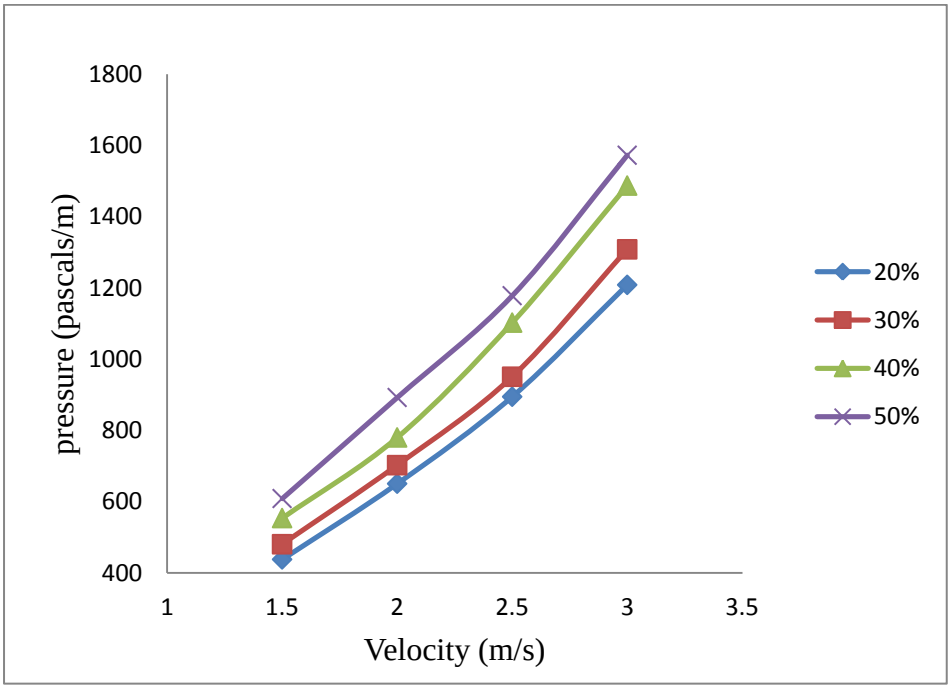

Fig 4.3(b): Pressure variation in straight pipe with 8:2(B.A:F.A)

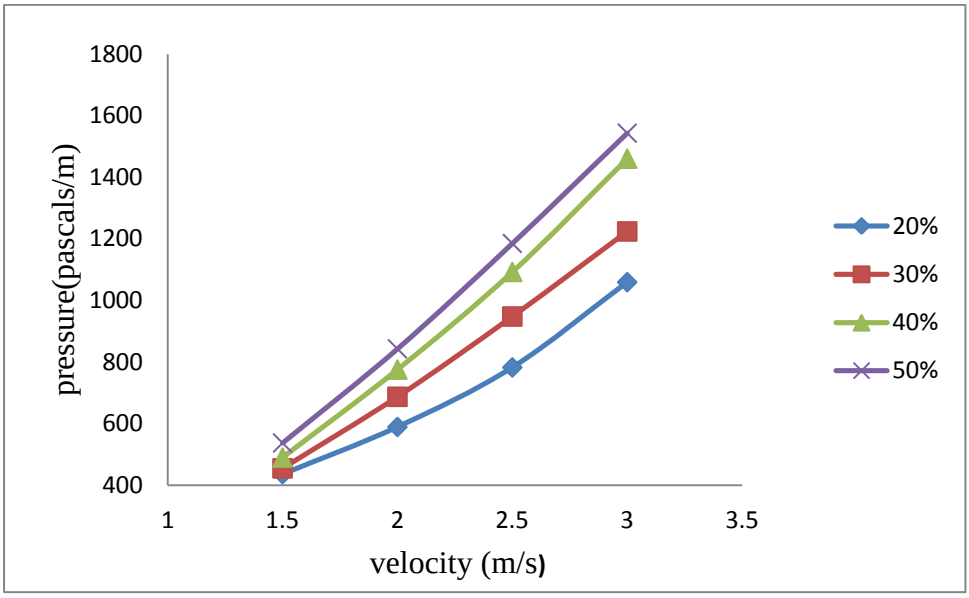

Fig 4.3 (c): Pressure variation of B.A with 4% additive (sodium bicarbonate) for straight pipe

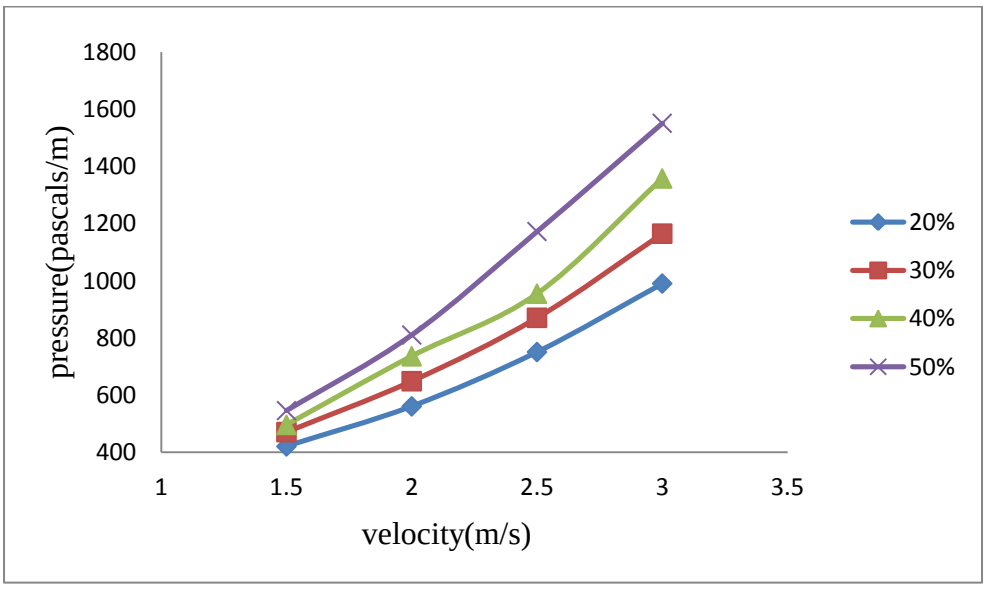

Fig 4.3(d): Pressure variation of B.A with 6 % additive (sodium bicarbonate) for straight pipe

Fig 4.3(a)-(d) shows that pressure loss at less concentrations is less as compared to pressure loss at high concentrations. Pressure drop increases as the concentration of solids increases and also increases with the increase of flow velocity. From the mentioned figures it can be also concluded that pressure drop at low concentrations with Bottom ash and additive mixture shows less pressure drop as compared with bottom and fly ash mixtures.

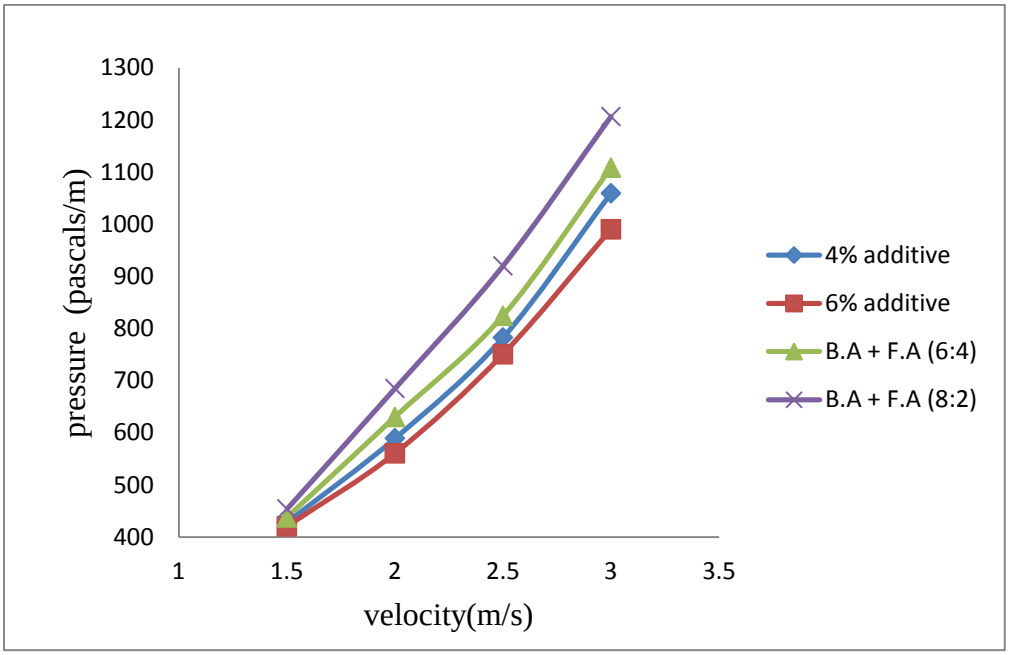

Fig 4.4 (a): Pressure variation of B.A + F.A ratios and bottom ash with additive (sodium bicarbonate) at 20% concentration (by weight)

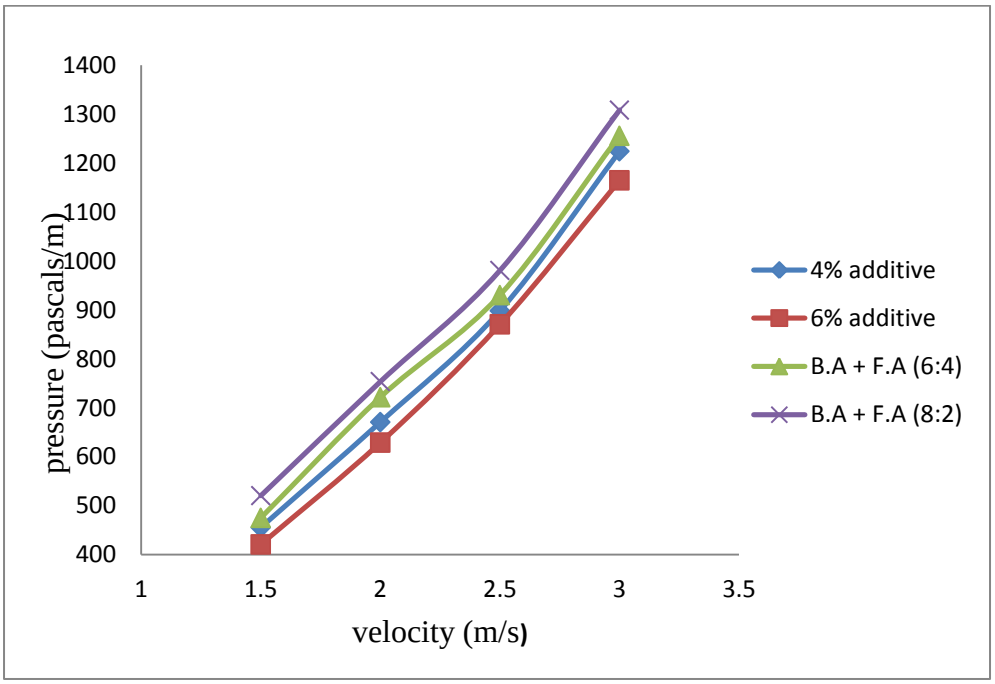

Fig 4.4 (b): Pressure variation of B.A + F.A ratios and bottom ash with additive (sodium bicarbonate) at 30% concentration (by weight)

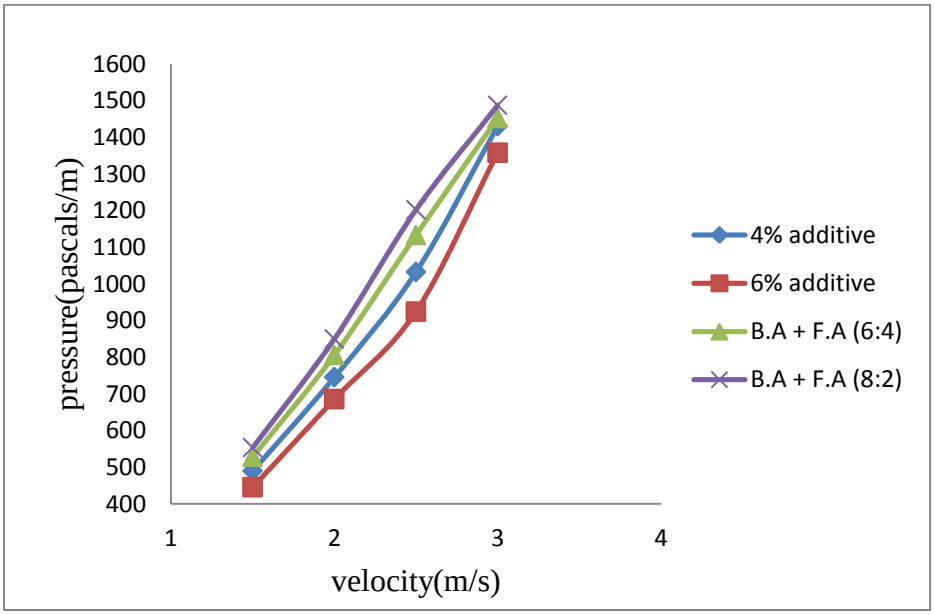

Fig 4.4 (c): Pressure variation of B.A + F.A ratios and bottom ash with additive (sodium bicarbonate) at 40% concentration (by weight)

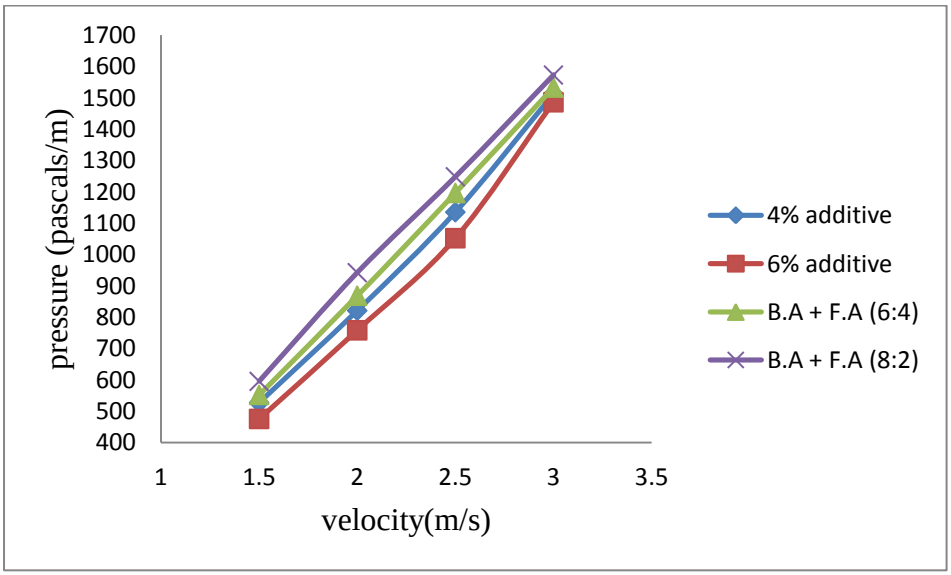

Fig 4.4 (d) Pressure variation of B.A + F.A ratios and bottom ash with additive (sodium bicarbonate) at 50% concentration (by weight)

Fig 4.4(a) - (d) shows that pressure drop variation is dependent also on weight percentage (%) of additive and ratio of B.A + F.A ratios. Mentioned figures clearly shows that at each concentration, bottom ash with 6% additive has least relative pressure increase and B.A + F.A (8:2) exhibits more pressure drop than other ash mixtures.

4.5 90^0 HORIZONTAL BEND MODELING

Model of 90^0 horizontal bend is created in the gambit version 2.2. Fig 4.5(a) shows the three dimensional model of pipe bend.

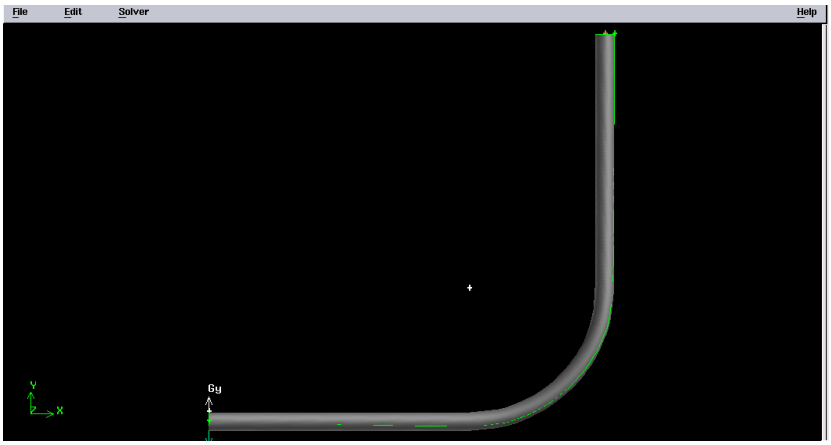

Fig 4.5(a): Three dimensional model of 90^0 horizontal bend

4.5.1 Grid independency test : Meshing of 90^0 horizontal bend with three different element sizes is done in Gambit version 2.2.Table 4.3 shows the parameters of meshing with different sizes.

Table 4.3 Mesh comparison for 90^0 horizontal bend

Element type	Element size	Elements	Skewness	Aspect Ratio
Mixed mesh	4	252642	0.74	2.95
Mixed mesh	5	197212	0.74	3.07
Mixed mesh	6	11586	0.74	2.98

Mesh size of 4 and mixed element type meshing is considered for further simulation. Fig 4.5(b) shows the meshed 90^0 horizontal bend.

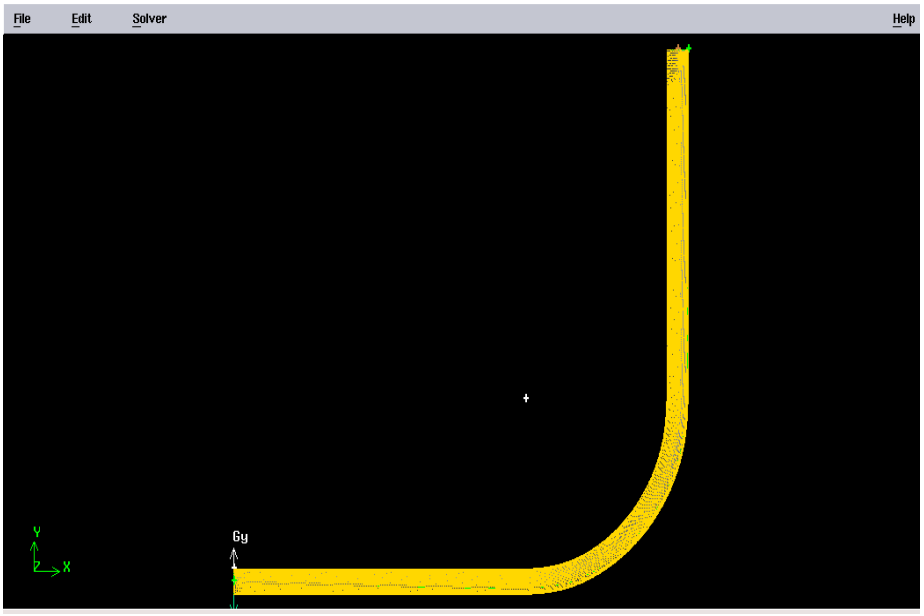

Fig 4.5(b): Meshed 90^0 horizontal bend

4.6 SIMULATION RESULTS OF 90^0 HORIZONTAL BEND

Fig 4.6 (a)-(d) shows the variation of pressure for different ratios of bottom and fly ash with different flow velocities and at different concentrations.

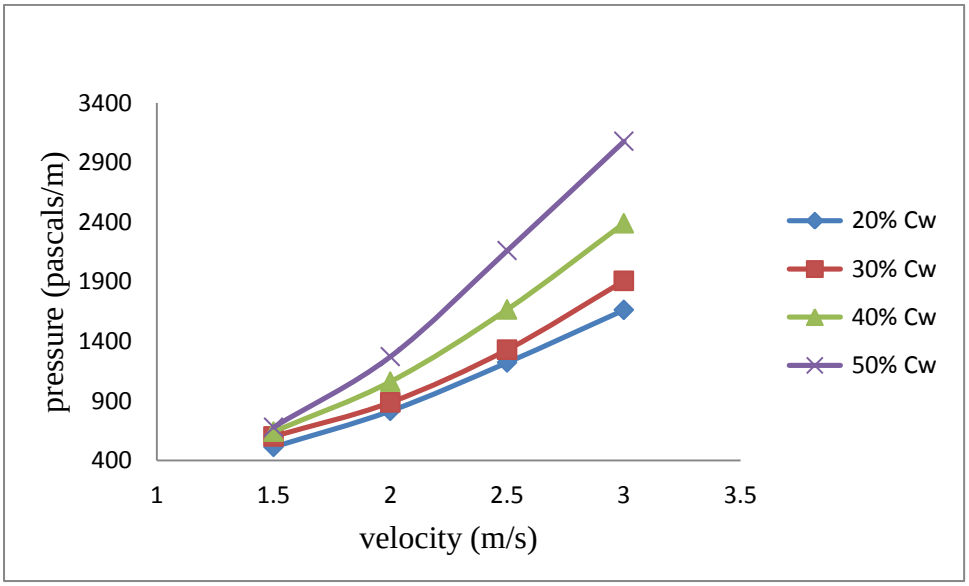

Fig 4.6 (a) : Pressure variation in 90^0 horizontal bend with B.A+F.A (6:4)

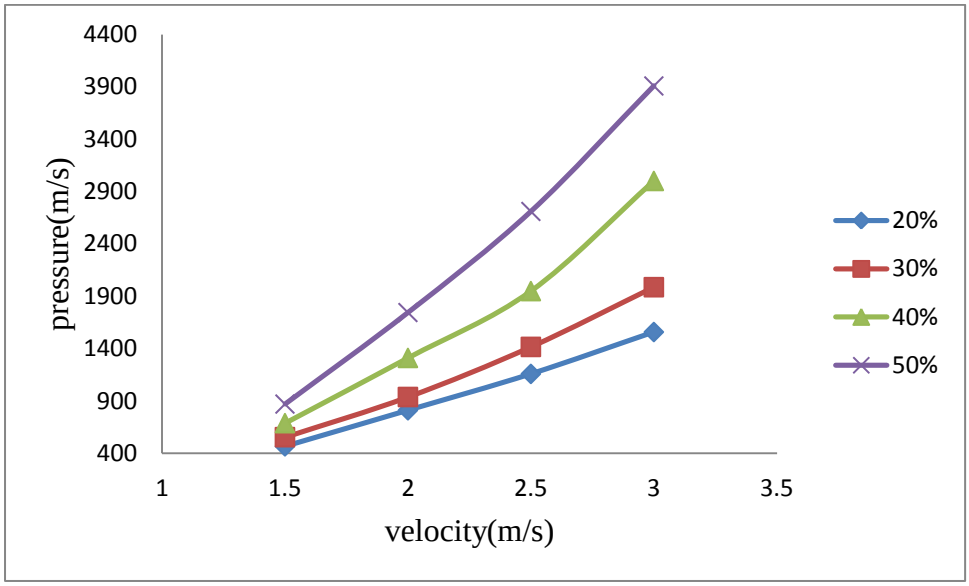

Fig 4.6 (b) : Pressure variation in 90^0 horizontal bend with B.A+F.A (8:2)

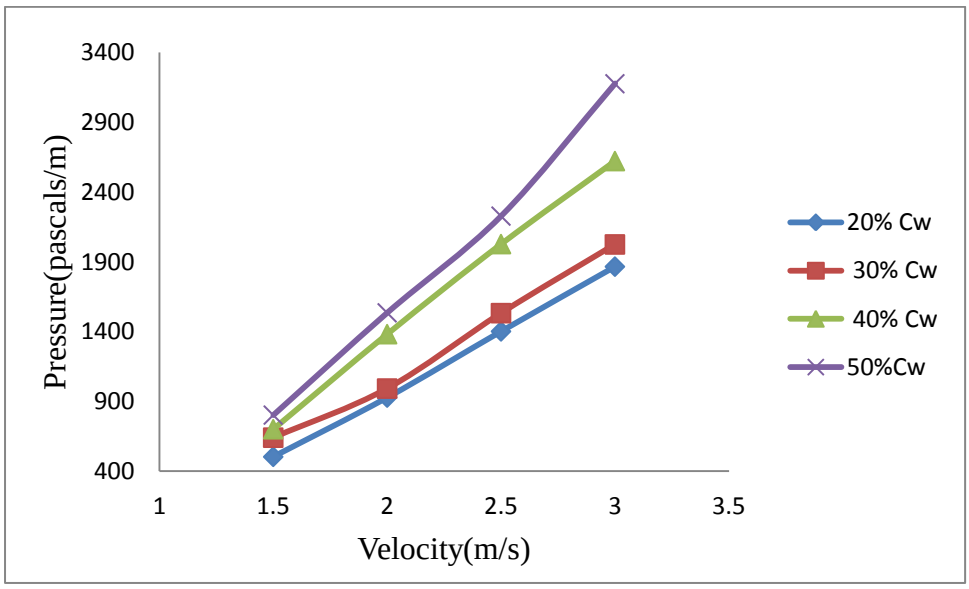

Fig 4.6 (c): Pressure variation in 90^0 horizontal bend with 4% additive (sodium bicarbonate) of bottom ash.

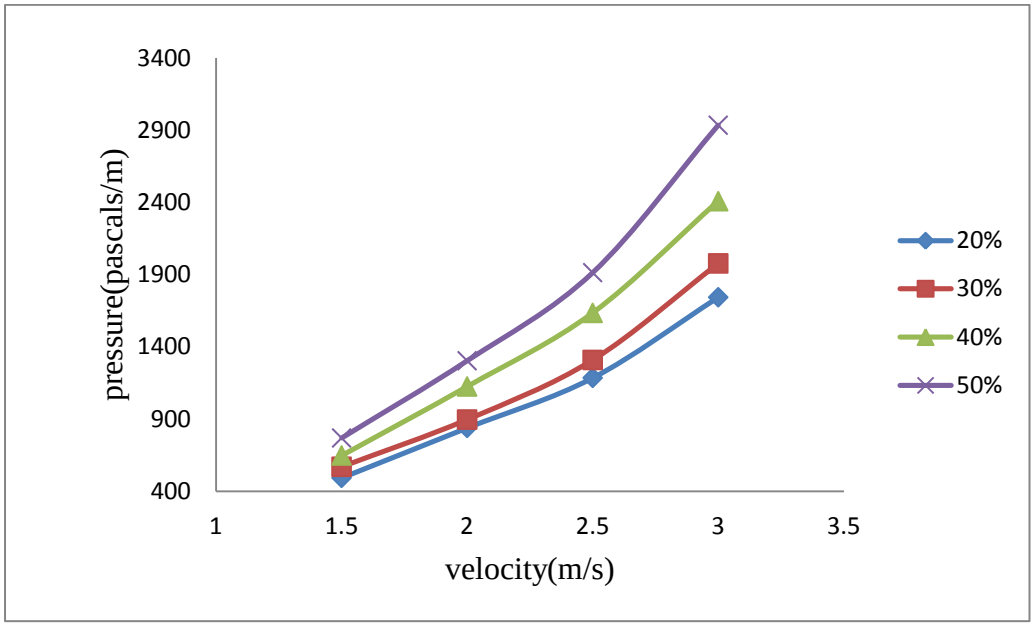

Fig 4.6(d): Pressure variation in 90^0 horizontal bend with 6% additive (sodium bicarbonate) in bottom ash.

Fig 4.6(a)-(d) shows that pressure drop in 90^0 horizontal bend increases with increasing concentration and flow velocity. It can be observed that pressure loss difference at high velocities is considerably more than pressure loss difference at low velocities.

Fig 4.7(a)-(d) shows the comparison of pressure variation of different ratio of bottom : fly ash and bottom ash with additive (sodium bicarbonate) at same concentration (by weight).

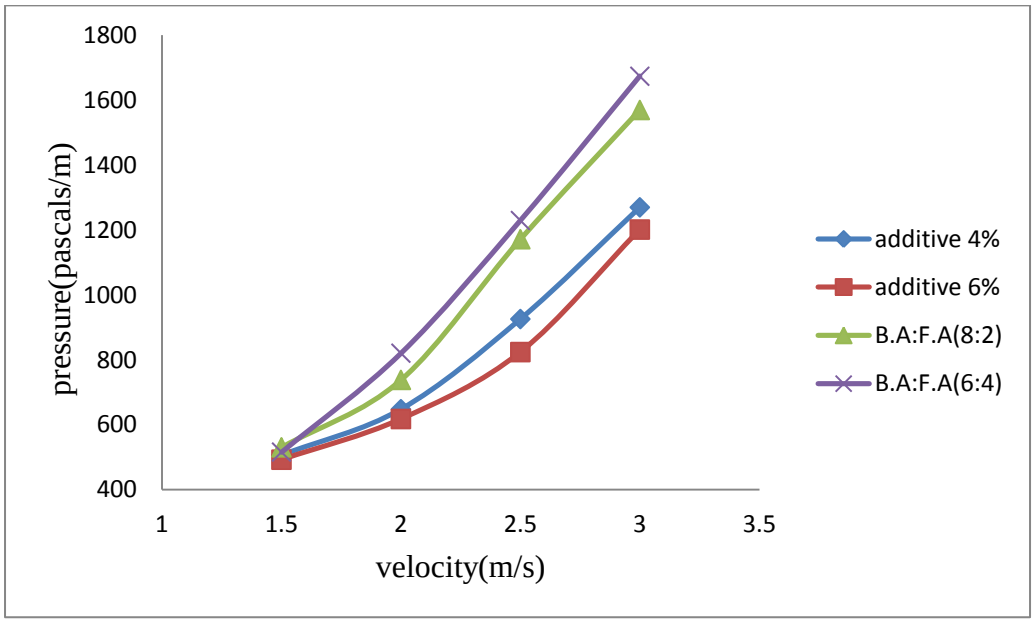

Fig. 4.7(a): Pressure variation of bottom and fly ash ratios and bottom ash with additive (sodium bicarbonate) for 20% concentration (by weight) of ash in 90^0 horizontal bend.

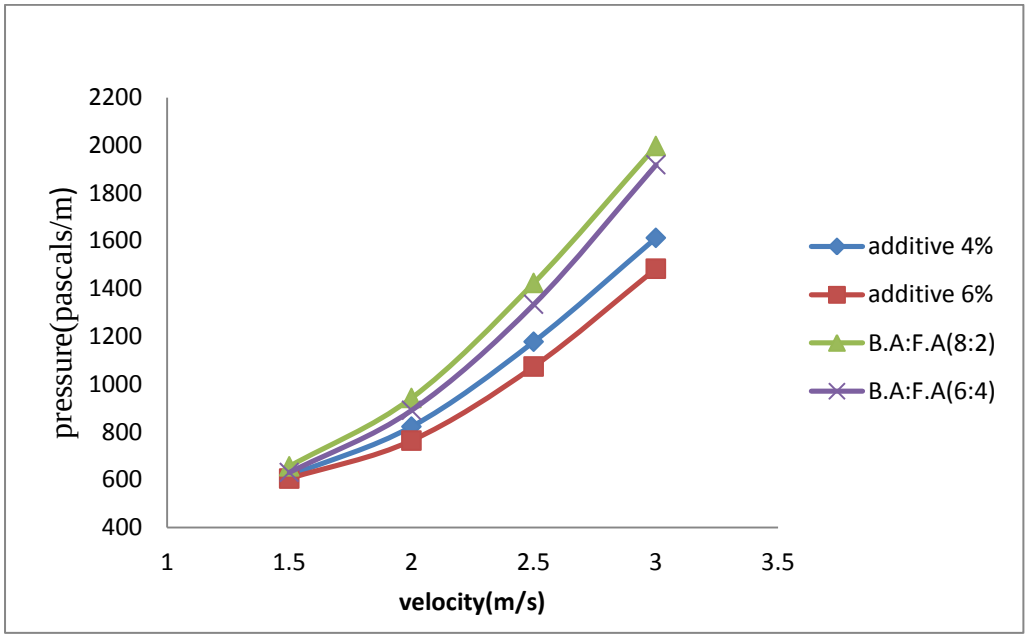

4.7(b): Pressure variation of bottom and fly ash ratios , bottom ash with additive (sodium bicarbonate) for 30% concentration (by weight) of ash in 90^0 horizontal bend.

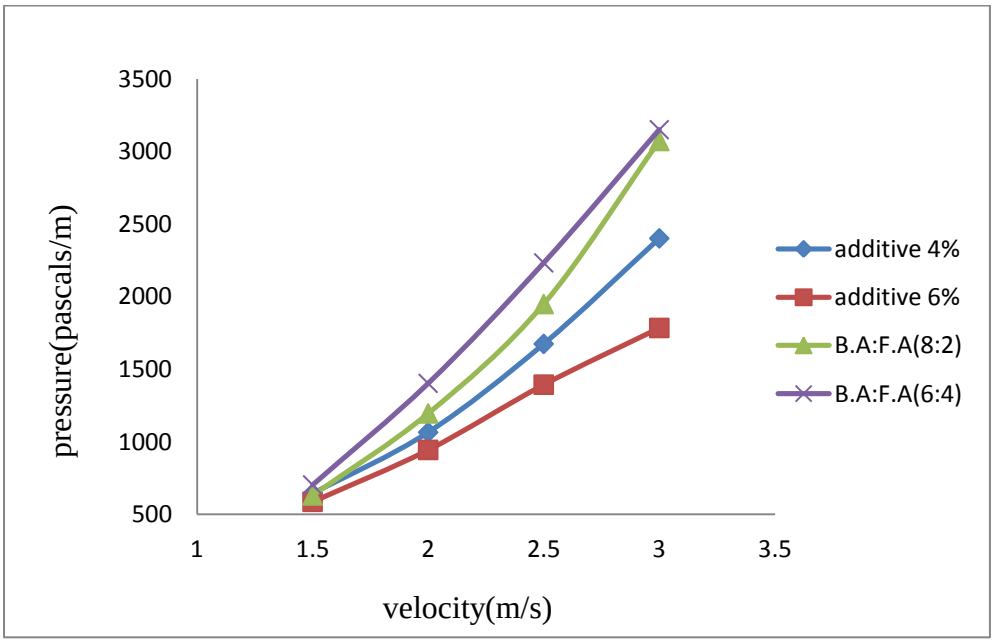

Fig:4.7(c): Pressure variation of bottom and fly ash ratios, bottom ash with additive (sodium bicarbonate) for 40% concentration (by weight) in 90^0 horizontal bend.

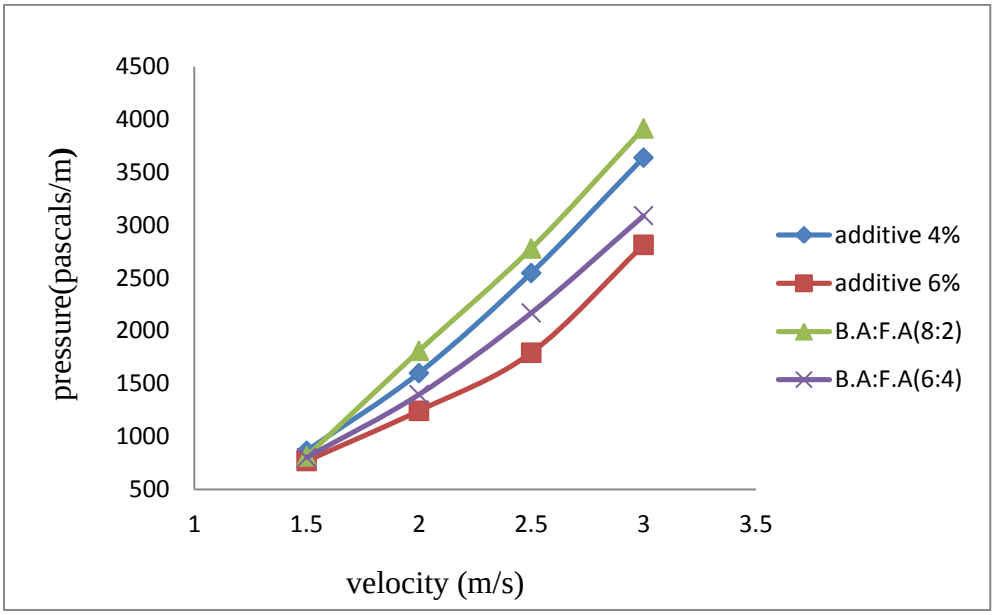

Fig 4.7(d): Pressure variation of bottom and fly ash ratios, bottom ash with additive (sodium bicarbonate) for 50% concentration (by weight) in 90^0 horizontal bend.

Fig 4.7(a)-(d) shows that bottom ash with 6% additive shows least increase in pressure drop at same concentration and B.A : F.A (8:2) shows maximum increase in pressure drop. It can be observed from the mentioned figures that pressure drop difference at low velocities for different ratios of bottom and fly ash is very less as compared to pressure drop difference at high velocities.

CHAPTER 5
CONCLUSION AND FUTURE SCOPE

Pressure distribution along the straight pipe and 90^0 horizontal bend is evaluated at various mixture with ratio 8:2,6:4 and additive(sodium bicarbonate)at concentrations (20%, 30%,40% and 50%) and flow velocity range of 1.5 - 3 m/s. The result is validated from the analytical formula (Darcy Weisbach Equation) for the pressure drop of water in straight pipe. Rheological properties of bottom and fly ash ratios are investigated using Rheometer. Physical characteristics of ash such as Particle size distribution, pH specific gravity and settling behaviour has also been studied. The simulation results are obtained with different mass flow velocity conditions and different concentrations. Based on the present investigation the following conclusions can be obtained

- Pressure drop per unit length across the straight pipe and horizontal bend increases as the flow velocity increases.
- Pressure drop per unit length across the straight pipe and horizontal bend at high concentrations is significantly higher than pressure drop at low concentrations and low flow velocity.
- Pressure drop per unit length in case of bottom ash with 6% additive is found relatively lower than other bottom and fly ash mixtures.
- Pressure drop across horizontal pipe bend is significantly higher than straight pipe.
- FLUENT results give the good agreement with analytical results for pressure drop in straight pipe for water and different slurry concentrations of bottom and fly ash ratios.

FUTURE SCOPE

- The computational approach can be used to simulate the similar work with different operating conditions.
- Study on same parameters can be evaluated using experimental test loop.

REFERENCES

[1] P.K. Senapati, B.K. Mishra, A."**Effect of solids volume fraction, particle size and hydrodynamic interactions"** Institute of Minerals & Materials Technology, (Council of Scientific & Industrial Research), Bhubaneswar-751 013, India Powder Technology 197 (2010) 1–8.

[2] Veruscha Fester, Baudouin Mbiya, Paul Slatter "**Energy losses of non-Newtonian fluids in sudden pipe**" ,Chemical Engineering Journal 145 (2008) 57–63

[3] Kaushal D.R. and Tomita Y, (2002), "**Solids concentration profiles and pressure drop in pipeline flow of multisized particulate slurries**", International Journal Multiphase Flow, Vol 28, pp. 1697-1717.

[4] A.M.Rebeiro & T.R.Bott, "**The influence of bend on drop sizes in horizontal annular two phase flow**", International journal of multiphase flow(2001) 721-728.

[5] Jure Marn, Primož Ternik, "**Laminar flow of a shear-thickening fluid in a 90^0pipe bend**", Fluid Dynamics Research 38 (2006) 295–312.

[6] J.Schmidt,L.Freidal, "**Two phase pressure drop across sudden contraction ducts",International journal of multiphase flow**,Vol 23 no.2, pp 283-299,1997.

[7] L. Mika, "**Energy losses of ice slurry in pipe sudden contractions**", Experimental Thermal and Fluid Science 35 (2011) 939–947.

[8] D.R. Kaushal , V. Seshadri , S.N. Singh, "**Prediction of concentration and particle size distribution in the flow of multi-sized particulate slurry through rectangular duct**", Applied Mathematical Modelling 26 (2002) 941–952.

[9] T. Balakhrisna, S. Ghosh , G. Das , P.K. Das, "**Oil–water flows through sudden contraction and expansion in a horizontal pipe – Phase distribution and pressure drop**", International Journal of Multiphase Flow 36 (2010) 13–24

[10] Chi-Chuan Wang, Chih-Yung Tseng, Ing Youn Chen, " **A new correlation and the review of two-phase flow pressure change across sudden expansion in small channels**", International Journal of Heat and Mass Transfer 53 (2010) 4287–4295.

[11] D.M. Binding , P.M. Phillips , T.N. Phillips, "**Contraction/expansion flows: The pressure drop and related issues**" J. Non-Newtonian Fluid Mech. 137 (2006) 31–38.

[12] Wael H. Ahmed, Chan Y. Ching , Mamdouh Shoukri, "**Pressure recovery of two-phase flow across sudden expansions**", International Journal of Multiphase Flow 33 (2007) 575–594.

[13] Ing Youn Chen , Chih-Yung Tseng , Yur-Tsai Lin , Chi-Chuan Wang, "**Two-phase flow pressure change subject to sudden contraction in small rectangular channels**", International Journal of Multiphase Flow 35 (2009) 297–306.

[14] P.K. Senapati , B.K. Mishra, A. Parida , "**Modeling of viscosity for power plant ash slurry at higher concentrations: Effect of solids volume fraction, particle size and hydrodynamic interactions**" Powder Technology 197 (2010) 1–8.

[15] D.R. Kaushal , Kimihiko Sato , Takeshi Toyota ,Katsuya Funatsu , Yuji Tomita, "**Effect of particle size distribution on pressure drop and concentration profile in pipeline flow of highly concentrated slurry**" International Journal of Multiphase Flow 31 (2005) 809–823.

[16] Va´clav Matouxek, "**Research developments in pipeline transport of settling slurries**" Powder Technology 156 (2005) 43 – 51.

[17] Meng Liu, Yu Feng Duan, "**Resistance properties of coal–water slurry flowingthrough local piping fittings**" Experimental Thermal and Fluid Science 33 (2009) 828–837.

[18] A.Mukhtar,S.N.singh,V.Shishadri, "**Pressure drop in long radius 90^0 horizontal bend for the flow of multisized heterogeneous slurry**",International journal multiphase flow, Vol 21,no.2,pp 329 332,1995.

[19] F. Boylu, H. Dinc¸er, G. Ates¸ok "**Effect of coal particle size distribution, volume fraction and rank on the rheology of coal–water slurries**" Fuel Processing Technology 85 (2004) 241–250.

[20] R. Greenwood , P.F. Luckham , T. Gregory "**Minimising the viscosity of concentrated dispersions by using bimodal particle size distributions**" Colloids Surfaces A: Physicochem. Eng. Aspects 144 (1998) 139–147.

[21] C. Logos, Q.D. Nguyen "**Effect of particle size on the flow properties of a South Australian coal-water slurry**" Powder Technology 88 (1996) 55-58.

[22] Nam-Sun Roh, Dae-Hyun Shin, Dong-Chan Kim and Jong-Duk "**Rheological behaviour of coal-water mixtures 1. Effects of coal type, loading and particle size"**
Fuel 1995 Volume 74 , 8.

[23] Ahmet Gürses , Metin Açıkyıldız , Çetin Doğar , Semra Karaca , Ramis Bayrak
"An investigation on effects of various parameters on viscosities of coal–water mixture prepared with lignite coal" Fuel Processing Technology 87 (2006) 821–827.

[24] Raffi M. Turian*, Jamel F. Attal1, Dong-Jin Sung, Lewis E. Wedgewood "**Properties and rheology of coal–water mixtures using different coals**" Fuel 81 (2002) 2019–2033

[25] N. Mangesana, R.S. Chikuku, A.N. Mainza, I. Govender, A.P. van der Westhuizen, and M. Narashima "**The effect of particle sizes and solids concentration on the rheology of silica sand**

based suspensions" The Journal of The Southern African Institute of Mining and Metallurgy volume 108 non-refered paper APRIL 2008 page no.237.

[26] Liangyong Chen, Yufeng Duan **"CFD simulation of coal-water slurry flowing in horizontal pipelines"** Korean J. Chem. Eng., **26**(4), 1144-1154 (2009).

[27] D.R. Kaushal , T. Thinglas , Yuji Tomita , Shigeru Kuchii , Hiroshi Tsukamoto **" CFD modeling for pipeline flow of fine particles at high concentration**" International Journal of Multiphase Flow 43 (2012) 85–100.

[28] R. You , J.Peddieson , J.Gadiyaram,S.Munukutla "**Simulation of particle/fluid flows in vertical circular pipes**" International Journal of Non-Linear Mechanics 45 (2010) 490–506

[29] M. Rudman∗ , H.M. Blackburn, L.J.W. Graham, L. Pullum "**Turbulent pipe flow of shear-thinning fluids**" J. Non-Newtonian Fluid Mech. 118 (2004) 33–48

[30] M. Eesa, M. Barigou "**Horizontal laminar flow of coarse nearly-neutrally buoyant particles in non-Newtonian conveying fluids: CFD and PEPT experiments compared**" International Journal of Multiphase Flow 34 (2008) 997–1007

[31] Margherita Cadorin, Mirko Morini*, Michele Pinelli "**Numerical analyses of high Reynolds number flow of high pressure fuel gas through rough pipes**" international journal of hydrogen energy 35(2010)7568-7579.

[32] Sowjanya Vijiapurapu , Jie Cui , Sastry Munukutla "**CFD application for coal/air balancing in power plants**" Applied Mathematical Modelling 30 (2006) 854–866.

ANNEXURE 1

Table 1.1: Particle Size distribution of Fly ash.

Particle size, μm	355	300	250	212	180	150	125	90	75	53
% finer	100	99	98.5	97	95	92	88	80	69	48

Table 1.2: Particle size distribution of Bottom ash

Φ_m (μm)	% finer
Below 2000	100
1400	89.5
710	85.2
355	72.6
300	65
250	58.8
212	46.8
180	44.1
150	20.6
125	17.4
90	13.5
75	3

Table 1.3: Variation of pH with different solid concentration (by weight) of bottom ash and Fly ash.

C_w, %	0	20	25	30	35	40	45	50
pH of bottom ash	7.75	7.67	7.66	7.66	7.64	7.63	7.62	7.62
pH of fly ash	7.75	7.59	7.55	7.51	7.48	7.46	7.45	7.44

Table 1.4: Settling characteristics of Fly and Bottom ash with initial concentration of 20%

Time(minute)	% C_w Bottom Ash	% C_w Fly Ash
0	20	20
1	24.97	28.12
2	25.28	33.16
3	29.80	42.37
4	32.2	45.25
5	44.35	47.39
15	53.9	47.39
30	53.9	47.39
60	54.49	48.54
120	55.70	48.54
180	55.70	48.54
240	56.98	49.01
480	56.98	49.01

Table 1.5:Chemical composition analysis of the fly and bottom ash

Material		Chemical composition (by weight %)								
	CO_2	Al_2O_3	SiO_2	K_2O	CaO	TiO_2	FeO	CuO	ZnO	others
Fly ash	10.38	26.57	45.18	1.53	1.96	1.95	4.98	2.97	3.03	1.45
Bottom ash	2.33	33.03	51.54	0.70	1.87	4.02	4.34	1.11	1.05	0.01

Table 1.6: Shear rate vs Shear stress variation of 10%Concentratio(byweight) of bottom ash and different ratios of bottom and fly ash

shear rate	bottom ash 10%	FA+BA(9:1)	FA+BA(8:2)	FA+BA(7:3)	FA+BA(3:2)
(1/sec)	stress(pa)	stress(pa)	stress(pa)	stress(pa)	stress(pa)
0	0	0	0	0	0
50	0.048	0.048	0.0484	0.05	0.055
100	0.097	0.098	0.099	0.102	0.108
125	0.12	0.128	0.13	0.15	0.18
150	0.152	0.165	0.175	0.205	0.22
175	0.17	0.18	0.19	0.21	0.24
200	0.21	0.23	0.25	0.27	0.31
225	0.23	0.25	0.275	0.3	0.33
250	0.255	0.28	0.31	0.34	0.37
275	0.275	0.3	0.33	0.36	0.4
300	0.31	0.34	0.37	0.41	0.45

Table 1.7: Shear rate vs Shear stress variation of 20% Concentratio(byweight) of bottom ash and different ratios of bottom and fly ash

Shear rate	bottom ash 20%	FA+BA(9:1)	FA+BA(8:2)	FA+BA(7:3)	FA+BA(3:2)
(1/sec)	stress(pa)	stress(pa)	stress(pa)	stress(pa)	stress(pa)
0	0	0	0	0	0
50	0.067	0.067	0.069	0.07	0.075
100	0.145	0.16	0.176	0.188	0.2
125	0.18	0.195	0.21	0.239	0.25
150	0.21	0.235	0.25	0.286	0.3
175	0.25	0.27	0.29	0.31	0.34
200	0.3	0.33	0.35	0.37	0.4
225	0.33	0.37	0.395	0.42	0.46
250	0.36	0.39	0.42	0.455	0.48
275	0.4	0.424	0.45	0.49	0.56
300	0.44	0.46	0.49	0.6	0.74

Table 1.8: Shear rate vs Shear stress variation of 30% Concentratio(byweight)of bottom ash and different ratios of bottom and fly ash

shear rate	bottom ash 30%	FA+BA(9:1)	FA+BA(8:2)	FA+BA(7:3)	FA+BA(3:2)
(1/sec)	stress(pa)	stress(pa)	stress(pa)	stress(pa)	stress(pa)
0	0	0	0	0	0
50	0.11	0.15	0.18	0.19	0.21
100	0.23	0.27	0.28	0.28	0.31
125	0.28	0.34	0.36	0.39	0.43
150	0.335	0.395	0.42	0.45	0.48
175	0.415	0.48	0.52	0.53	0.59
200	0.445	0.55	0.6	0.65	0.69
225	0.5	0.59	0.6	0.72	0.78
250	0.52	0.61	0.65	0.8	0.86
275	0.605	0.69	0.74	0.89	0.92
300	0.69	0.76	0.8	0.95	1.03

Table 1.9: Shear rate vs Shear stress variation of 40% Concentratio(byweight) of bottom ash and different ratios of bottom and fly ash

shear rate	bottom ash 40%	FA+BA(9:1)	FA+BA(8:2)	FA+BA(7:3)	FA+BA(3:2)
(1/sec)	stress(pa)	stress(pa)	stress(pa)	stress(pa)	stress(pa)
0	0	0	0	0	0
50	0.16	0.2	0.25	0.31	0.37
100	0.26	0.33	0.39	0.48	0.53
125	0.39	0.45	0.54	0.62	0.67
150	0.43	0.5	0.58	0.64	0.74
175	0.54	0.6	0.67	0.75	0.85
200	0.61	0.67	0.73	0.8	0.91
225	0.68	0.77	0.85	0.93	1.03
250	0.77	0.84	0.92	0.98	1.08
275	0.89	0.96	1.05	1.13	1.19
300	0.98	1.1	1.19	1.3	1.45

Table 1.10: Shear rate vs Shear stress variation of 50% Concentratio(byweight) of bottom ash and ratios of bottom and fly ash

shear rate	bottom ash 50%	FA+BA(9:1)	FA+BA(8:2)	FA+BA(7:3)	FA+BA(3:2)
(1/sec)	stress(pa)	stress(pa)	stress(pa)	stress(pa)	stress(pa)
0	0	0	0	0	0
50	0.23	0.31	0.37	0.44	0.53
100	0.48	0.54	0.64	0.72	0.81
125	0.58	0.68	0.79	0.86	0.95
150	0.7	0.81	0.93	1	1.1
175	0.76	0.92	1.03	1.15	1.25
200	0.92	1.07	1.17	1.3	1.5
225	1.04	1.16	1.26	1.4	1.6
250	1.17	1.27	1.39	1.7	1.9
275	1.35	1.4	1.52	1.75	2
300	1.495	1.61	1.74	1.9	2.3

ANNEXURE 2

Table 2.1: Pressure drop per unit length with different flow velocity and % concentration(by weight) for B.A:F.A (8:2) mixture in straight pipe

Velocity (m/s)	Pressure drop (pascals/m) in 20%	Pressure drop (pascals/m) in 30%	Pressure drop (pascal/m)in 40%	Pressure drop (pascals/m) in 50%
1.5	437.8	480.34	513.8	556.71
2	650.45	702.34	780.28	862.43
2.5	894.63	950.67	1002.668	1178.28
3	1178.63	1232.39	1387.47	1542.65

Table 2.2: Pressure drop per unit length with different flow velocity and %concentration(by weight for B.A:F.A (6:4) mixture in straight pipe

Velocity (m /s)	Pressure drop (pascals/m) in 20%	Pressure drop (pascals/m) in 30%	Pressure drop (pascals/m) in 40%	Pressure drop (pascals/m) in 50%
1.5	434.27	464.9	528.64	587.48
2	685.25	741.47	806.33	898.75
2.5	920.28	982.3	1092.69	1236.6
3	1206.66	1255.8	1412.43	1552.75

Table 2.3: Pressure drop per unit length with different flow velocity and % concentration(by weight) for B.A with 4%additive(sodium bicarbonate) in straight pipe

Velocity (m/s)	Pressure drop (pascals/m) in 20%	Pressure drop (pascals/m) in 30%	Pressure drop (pascals/m) in 40%	Pressure drop (pascals/m) in 50%
1.5	436.5	455.23	490.56	537.74
2	589.67	687.62	776	843.32
2.5	782.84	948.2	1062.9	1185.37
3	1059.6	1224.23	1460.56	1523.45

Table 2.4: Pressure drop per unit length with different flow velocity and % concentration(by weight) for B.A with 6% additive(sodium bicarbonate) in straight pipe

Velocity(m/s)	Pressure drop (pascals/m) in 20%	Pressure drop (pascals/m) in 30%	Pressure drop (pascals/m) in 40%	Pressure drop (pascals/m) in 50%
1.5	420.7	470.61	495.82	545.79
2	560.7	648.74	735.96	810.48
2.5	750.78	870.52	954.7	1172.29
3	990.42	1164.8	1357.93	1510.91

Table 2.5: Pressure drop per unit length with different flow velocity and % concentration(by weight) for B.A:F.A (6:4) mixture in 90^0 bend

Velocity(m/s)	Pressure drop (pascals/m) in 20%	Pressure drop (pascals/m) in 30%	Pressure drop (pascals/m) in 40%	Pressure drop (pascals/m) in 50%
1.5	513.02	554.45	688.25	870.30
2	831.09	937.79	1310.96	1744.54
2.5	1258.5	1416.20	1949.39	2709.88
3	1578.22	1986.41	3000.96	3908.19

Table 2.6: Pressure drop per unit length with different flow velocity and % concentration(by weight) for B.A:F.A (8:2) mixture in 90^0 bend

Velocity (m/s)	Pressure drop (pascals/m) in 20%	Pressure drop (pascals/m) in 30%	Pressure drop (pascals/m) in 40%	Pressure drop (pascals/m) in 50%
1.5	495.19	534.65	641.144	678.37
2	815.51	886.38	1060.55	1270.56
2.5	1121.76	1328.73	1666.56	2161.14
3	1562.71	1906.68	2389.83	3078.54

Table 2.7: Pressure drop per unit length with different flow velocity and % concentration(by weight) for B.A 6% additive(sodium bicarbonate) in 90^0 bend.

Velocity (m/s)	Pressure drop (pascals/m) in 20%	Pressure drop (pascals/m) in 30%	Pressure drop (pascals/m) in 40%	Pressure drop (pascals/m) in 50%
1.5	492.59	569.21	647.36	768.67
2	838.61	896.29	1125.21	1303.61
2.5	1184.94	1308.83	1634.81	1913.43
3	1523.01	1677.33	2408.06	2934.27

Table 2.8: Pressure drop per unit length with different flow velocity and % concentration(by weight) for B.A 4% additive(sodium bicarbonate) in 90^0 bend.

Velocity(m/s)	Pressure drop (pascals/m) in 20%	Pressure drop (pascals/m) in 30%	Pressure drop (pascals/m) in 40%	Pressure drop (pascals/m) in 50%
1.5	503.8494	640.9639	701.488	802.7108
2	928.1807	992.5723	1382.38	1535.241
2.5	1402.133	1382.651	2027.349	2227.892
3.5	1545.867	1788.759	2621.988	3175.843

ANNEXURE 3

Table 3.1: Pressure drop increase in bend per unit length with different flow velocity and 20 % concentration(by weight) for B.A:F.A (8:2) mixture

	straight pipe	Pipe bend	
Velocity (m/s)	Pressure Drop(pascals)	Pressure Drop(pascals)	% Increase
1.5	437.8	495.19	13.10873
2	650.45	815.51	25.37628
2.5	894.63	1152.76	28.38815
3	1178.63	1562.71	32.58699

Table 3.2: Pressure drop increase in bend per unit length with different flow velocity and 30 % concentration(by weight) for B.A:F.A (8:2) mixture

	straight pipe	Pipe bend	
Velocity (m/s)	Pressure Drop(pascals)	Pressure Drop(pascals)	% Increase
1.5	480.34	534.65	11.306575
2	702.34	886.38	26.203833
2.5	950.67	1328.73	39.767743
3	1232.39	1906.68	54.714011

Table 3.3: Pressure drop increase in bend per unit length with different flow velocity and 20 % concentration(by weight) for B.A:F.A (6:4) mixture

	straight pipe	Pipe bend	
Velocity (m/s)	Pressure Drop(pascals)	Pressure Drop(pascals)	% Increase
1.5	434.27	513.02	18.13388
2	685.25	831.09	21.28274
2.5	920.28	1258.5	36.75186
3	1206.66	1578.22	30.79244

Table 3.4: Pressure drop increase in bend per unit length with different flow velocity and 30 % concentration(by weight) for B.A:F.A (6:4) mixture

	straight pipe	Pipe bend	
Velocity (m/s)	Pressure Drop(pascals)	Pressure Drop(pascals)	% Increase
1.5	464.9	554.45	19.262207
2	741.47	937.79	26.477133
2.5	982.3	1416.2	44.171842
3	1255.8	1986.41	58.17885

Table 3.5: Pressure drop increase in bend per unit length with different flow velocity and 20 % concentration(by weight) for B.A 6% additive(sodium bicarbonate)

	straight pipe	Pipe bend	
Velocity (m/s)	Pressure Drop(pascals)	Pressure Drop(pascals)	%Increase
1.5	420.7	492.59	17.08819
2	560.7	838.61	49.56483
2.5	750.78	1134.94	51.12786
3	990.42	1523.01	53.77416

Table 3.6: Pressure drop increase in bend per unit length with different flow velocity and 30 % concentration(by weight) for B.A 6% additive(sodium bicarbonate)

	straight pipe	Pipe bend	
Velocity (m/s)	Pressure Drop(pascals)	Pressure Drop(pascals)	% Increase
1.5	470.61	569.21	20.951531
2	648.74	896.29	38.158584
2.5	870.52	1308.83	50.350365
3	1164.8	1677.33	44.001545

Table 3.7: Pressure drop increase in bend per unit length with different flow velocity and 20 % concentration(by weight) for B.A 4% additive(sodium bicarbonate)

	straight pipe	Pipe bend	
Velocity (m/s)	Pressure Drop(pascals)	Pressure Drop(pascals)	% Increase
1.5	436.5	503.8494	15.42942
2	589.67	868.1807	47.23162
2.5	782.84	1162.133	48.4509
3	1059.6	1595.867	50.61032

Table 3.8: Pressure drop increase in bend per unit length with different flow velocity and 30 % concentration(by weight) for B.A 4% additive(sodium bicarbonate)

	straight pipe	Pipe bend	
Velocity (m/s)	Pressure Drop(pascals)	Pressure Drop(pascals)	% Increase
1.5	475.23	640.9639	34.874461
2	687.62	992.5723	44.348957
2.5	948.2	1382.651	45.818498
3	1224.23	1788.759	46.112985